A MULTISCALE ANALYSIS OF BLAST IMPACT MITIGATION ON THE HUMAN HEAD

by

DANIEL BRYAN JENSON

VINU UNNIKRISHNAN, COMMITTEE CHAIR
SAMIT ROY
NIMA MAHMOODI

A THESIS

Submitted in partial fulfillment of the requirements for the degree of
Master of Science in the Department of Aerospace Engineering and
Mechanics in the Graduate School of
The University of Alabama

TUSCALOOSA, ALABAMA

2014

ABSTRACT

The effectiveness of helmets in preventing shrapnel wounds and internal damage due to blast shock waves has been studied. Carbon nanotubes and similar nanostructures have also recently generated heightened interest due to their strength-to-weight ratio and other unique properties. Therefore, to understand and develop a helmet with improved protection, it is necessary to develop computational procedures that will enable the accurate modeling of traumatic head injuries as well as the precise measurement of the mechanical properties of nanostructures and how these characteristics behave when embedded as an advanced composite structure into a helmet. In this study, a multiscale simulation strategy is used to estimate the mechanical characteristics of advanced composite structures with embedded nanostructures.

In most of the previous theoretical works, an analysis dedicated to improving the design of the helmet using composite structures was not included due to a lack of understanding of the interactions of the nanostructures with the matrix materials. In this work, the role of the helmet on the over pressurization and impulse experienced by the head during blast shock wave and blunt force trauma due to shrapnel impacts is studied. In addition, the properties of nano-composite structures are estimated using molecular dynamics (MD) simulations and then scaled to the macroscopic level using continuum mechanic formulations. This modeling is further developed using Finite Element (FE) analysis to demonstrate the effectiveness of various types of nanostructures in energy absorption. An analysis is carried out on a model of an unprotected head to compare the results to those obtained when protected by a helmet containing different nanostructures. The developed multiscale model is used to improve the composition of helmets and the general understanding of the effects of blast shock wave and shrapnel impacts thereby leading to the mitigation and prevention of traumatic head injuries.

DEDICATION

This thesis is dedicated to my beautiful wife and to our patient children. They sacrificed much to allow me to be able to live my dream.

LIST OF ABBREVIATIONS AND SYMBOLS

Abbreviations:

ACH	Advanced Combat Helmet
bTBI	Blast induced traumatic brain injury
C3D4	4-Node Linear Tetrahedron Element
C3D8R	8-Node Linear Reduced Integration Brick Element
ConWep	Conventional Weapons Effects
CNT	Carbon Nanotube
CT	Computed Tomography
CSF	Cerebrospinal fluid
DICOM	Digital Imaging and Communications in Medicine
ECH	Enhanced Combat Helmet
EOS	Equation of State
FE	Finite Element
GCS	Glasgow Coma Scale
IED	Improvised Explosive Device
IEEE	Institute of Electrical and Electronics Engineers
K	Bulk Modulus of Elasticity
LWH	Lightweight Helmet
MD	Molecular Dynamics
MRE	Magnetic Resonance Elastography

MRI	Magnetic Resonance Imaging
M-T	Mori-Tanaka
Pa	Pascal
RVE	Representative Volume Element
.stl	STereoLithography
TNT	Trinitrotoluene
UHMWPE	Ultra-High Molecular Weight Polyethylene
W	Strain Energy Potential

Symbols:

A	Johnson-Cook coefficient
B	Johnson-Cook coefficient
β_i	Decay Constant
C	Johnson-Cook coefficient
c_0	Hugoniot Material Constant
C_{10}	Mooney-Rivlin Material Constant
C_{01}	Mooney-Rivlin Material Constant
D_1	Mooney-Rivlin Material Constant
$\dot{\varepsilon}$	Strain rate
$\dot{\varepsilon}_{ij}$	Deviatoric Strain Rate
E	Young's modulus
E_{kl}	Green's Strain Tensor
E_m	Hugoniot Material Constant
F	Deformation Gradient Tensor
G_i	Relaxation Modulus
$G_{ijkl}(t-\tau)$	Relaxation Modulus Function
Γ	Grüneisen Ratio
H	Hugoniot Material Constant
J	Jacobian of Transformation
J_1	First Invariant of the Deviatoric Strain

J_2	Second Invariant of the Deviatoric Strain
J_{el}	Elastic Volume Ratio
n	Johnson-Cook coefficient
ν	Poisson's Ratio
m	Johnson-Cook coefficient
μ	Shear Modulus of Elasticity
P	Pressure
$\dot{p}$	Pressure Rate
ρ_0	Density
S	Hugoniot Material Constant
σ	Stress
S_{ij}	Second Piola-Kirchhoff Stress

ACKNOWLEDGEMENTS

I would like to thank the professors at the University of Alabama who have helped me pursue my education in Aerospace Engineering. Specifically, I am very grateful for the assistance of Dr. Vinu Unnikrishnan, for his patience and diligence in teaching me how to write technical papers and perform research responsibilities. I am grateful for the time and effort he put into editing my thesis. I also appreciate the insight of my committee members, Dr. Samit Roy and Dr. Nima Mahmoodi. Also, this thesis would have been nearly impossible without the loving support of my family and friends.

CONTENTS

LIST OF TABLES

LIST OF FIGURES

CHAPTER ONE – INTRODUCTION

A soldier goes to the field anticipating attack. In the best scenarios, a soldier will not be subjected to ballistic impacts or blast shock waves from projectiles and explosives. The ballistic impacts caused by shrapnel and bullets cause traumatic brain injury. The explosions which generate shrapnel also create blast waves which can cause mild, moderate, or severe traumatic brain injury to soldiers and civilians. Improvised explosive devices (IEDs) are weapons which are utilized by insurgents during warfare. The utilization of a helmet does reduce the risk of ballistic impacts, but does not always remove the risk associated with shrapnel or blast waves. Blast-induced traumatic brain injury (bTBI) is a phenomenon dominated by stress waves compared to other impact injuries such as sports or automotive injuries. Possibly because of advances in helmets and other protective gear, many more soldiers impacted by shrapnel are surviving their injuries. However, the subsequent damage from the blast shock wave and its role in inducing traumatic brain injury is lacking in the scientific community. This work provides a study of multiscale approaches in the understanding of prevention and mitigation of blast shock wave injuries to the brain through the use of ballistic helmet design using novel materials.

Blast injury is caused by a sudden increase in air pressure and causes injuries in spaces containing gas [1]. In a blast, a shock wave forms which travels at the speed of sound. Air is accelerated by this shock wave, forming a high-velocity blast wind. This study is focused on the initial shock wave, to study the effects of the high-velocity winds [2]. Traumatic brain injury is induced by external mechanical forces, in this case, a blast shock wave, which is known as blast induced traumatic brain injury.

In the remainder of this work, the effect of the helmet on mitigating the effects of blast traumatic brain injury is studied. The second chapter contains a literature review outlining what has been studied and researched in the past. This review provides insight into what is lacking in the current knowledge of the effects of blast shock waves and their interactions with the human head and possible helmet protection systems. Chapter three is a discussion of some of the methods given in the literature for the study of blast traumatic brain injury. It describes what has been chosen as a guideline for this work. It also describes some of the important concepts used in modeling blast and creating a head-helmet model. These concepts include the representation of the blast wave using the Friedlander equation for estimating blast impact incident pressure, the Mooney-Rivlin hyperelastic model for simulating brain properties, and the Mori-Tanaka method for the homogenization of porous microstructures. Chapter four contains two parts. The first part discusses a simulation performed on a steel plate. The purpose of this part is to demonstrate the computational methodology in performing blast impact analysis on a simple model by comparing the results to those obtained in various experimental efforts obtained from literature. Other materials are also incorporated into the plate model, to perform preliminary tests on possible materials that could be better in mitigating blast shock wave impacts. In the subsequent part of chapter four, the head model is subjected to blast impacts and comparisons are made between a head protected by a helmet and an unprotected head. These results are also compared to the literature for validity. Various materials for the improvement of the helmet in mitigating blast shock wave impacts are also tested using the same model with different material properties. The results obtained from the simulations using new material properties are compared to those obtained with the unchanged helmet material properties. Chapter five marks the conclusion of

this analysis. It summarizes the findings contained throughout the analysis and suggests future work to be performed in this area of research.

CHAPTER TWO – LITERATURE SURVEY OF BLAST IMPACT MITIGATION

2.1 Abstract

The study of the effects of blast induced traumatic brain injury has recently received tremendous attention due to the high incidence on soldiers returning from the battlefield. This chapter contains a detailed literature review outlining the state of the art research in the study of bTBI and its mitigation strategies developed over the years. The study of blast traumatic brain injury involves experimental and numerical simulations, as well as understanding of the mechanics of bTBI, which involves not just the characterization of the blast but also having an accurate representation of the material properties involved. This review provides insight into the limitations of the current techniques in understanding the effects of blast waves and their interactions with the human head and development of possible remedial measures using helmet protection systems.

2.2 Blast Impact Experiments

Blast impacts are caused by a blast shock wave impacting the solid body. A blast wave is normally caused by high-order explosives caused by accidental explosions or bomb blasts. There have been two widely used experimental techniques used to study shock loading. The first method uses explosives to impart shock directly to the body, while the second method uses shock tubes to impart the shock loading. In a shock tube, planar wave fronts and other wave parameters are easy to control and study [3]. Since most blast impacts will not be planar waves in actual situations, a comparison with real explosives will be used to supply the supporting experimental data. Alley et al utilized an explosive driven shock tube to obtain experimental data, thus

combining shock tubes and explosives to allow for a focused pressure wave from an explosion [4]. The results for pressure were obtained using a model of the human skull and brain made from various polymers which had similar mechanical properties to the human skull and brain. Figure 2.1 demonstrates the shock tube method of studying blast impacts. The pressure wave travels through the tube until it impacts the specimen.

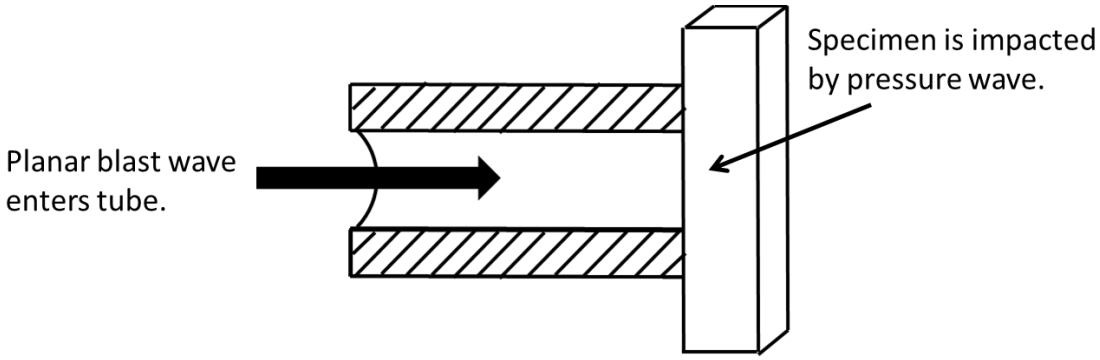

Figure 2.1: Shock tube experiment.

2.3 Traumatic Brain Injury

Traumatic brain injury, also called intra-cranial injury, is the damage to the brain caused by external mechanical forces and can cause permanent or temporary brain damage. Blast induced traumatic brain injury occurs when a blast wave causes traumatic brain injury (see Figure 2.2). There are other causes of traumatic brain injury which include automotive accidents, work related accidents, sporting injuries, and domestic violence, such as Shaken-Baby Syndrome etc. [2]. In young people, traumatic brain injury is the leading cause of disability and death. To grade the severity of traumatic brain injury, the Glasgow Coma Scale (GCS) score after resuscitation is usually used [5, 6]. This coma scale determines *mild* (GCS 13-15), *moderate* (GCS 9-13), and *severe* (GCS 3-8) traumatic brain injury. Table 2.1 shows the various indicators in the Glasgow Coma Scale. Mild traumatic brain injury is usually indicated by concussion and results in full neurological recovery, with some concentration and short-term memory problems.

Moderate traumatic brain injury leaves the patient lethargic, while severe traumatic brain injury results in a coma and an inability to open eyes or follow commands [5].

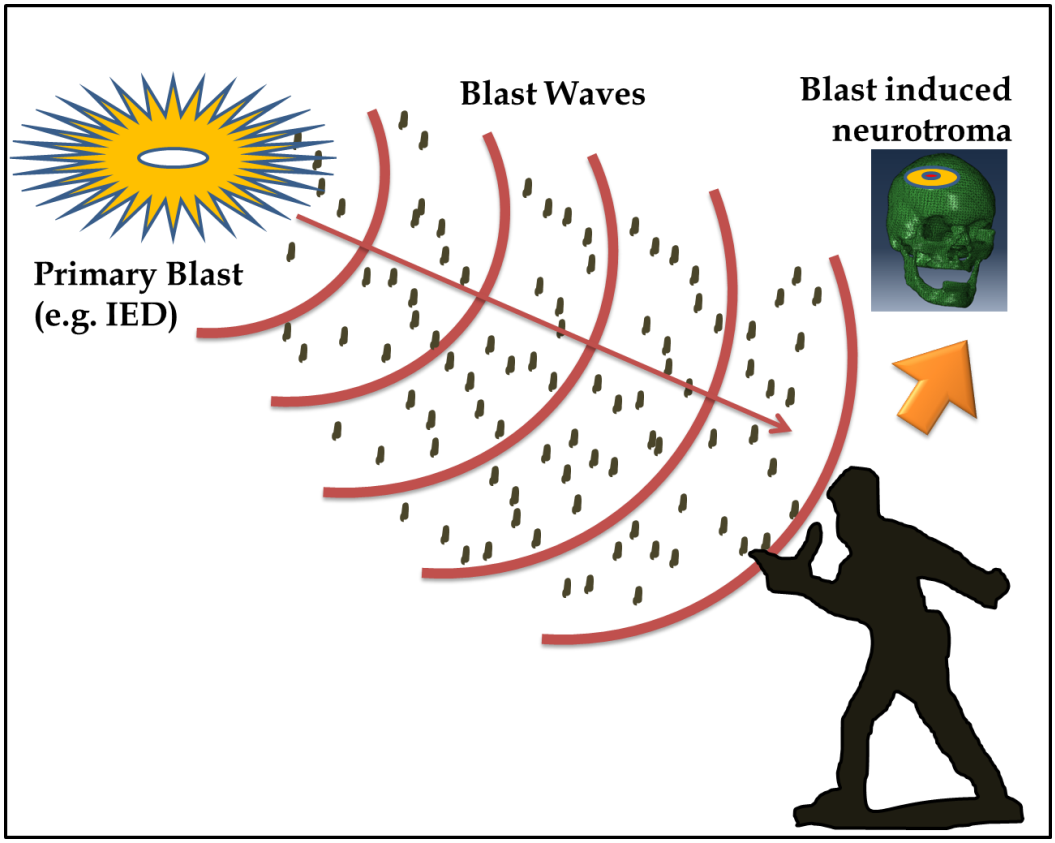

Figure 2.2: Blast induced traumatic brain injury (bTBI).

Table 2.1: Glasgow coma scale. Modified from [6].

Eye opening		**Motor response**		**Verbal response**	
Spontaneous	4	Obeys	6	Oriented	5
To speech	3	Localizes	5	Confused	4
To pain	2	Withdraws	4	Inappropriate	3
None	1	Abnormal flexion	3	Incomprehensible	2
		Extensor response	2	None	1
		None	1		

2.4 Causes of Blast Induced Traumatic Brain Injury

There are several causes of blast induced traumatic brain injury. Primary blast injury is caused by a high-pressure shock wave interacting with the body [2]. This shock wave produces

pressure which can be amplified due to the impedance mismatch between the skull and air [7]. The direct impact of the shock wave causes acceleration of the head, and since the inertia of the brain is less than the inertia of the skull, the brain continues vibrating after the skull has stopped. Cavitation bubbles are then formed from the intracranial pressure changes [2]. These bubbles cause injury to the brain when they collapse. In cases when the head is not directly subjected to the blast, the shock wave can be transferred through the abdomen to the blood vessels or other fluid pathways in the thoracic region. This compression effect can cause waves which transmit kinetic energy to the brain [8].

Another cause of traumatic brain injury is due to shrapnel and debris from explosions. This is called secondary blast injury, and can often go further than the primary high pressure blast wave. The acceleration of the different body parts by the blast wind can cause tertiary blast injuries as well. Due to the difference in inertia between the skull and brain, higher shearing strains form in the intra-cranial region, causing shearing injuries [2]. Further, the high pressure gases following the explosion are at very high temperatures and these hot gasses can cause quaternary injuries, which include pulmonary injuries from the toxic gas and burns. The brain is also damaged if the skull is heated excessively.

There are other problems also associated with exposure to a shock wave which has the potential to harm the brain. One such physiological effect is the compression of the air-carrying organs in the thorax and abdomen. This causes larger pressure in the intra-cranial region due to an increase in blood flow. An experiment to isolate the thoracic mechanism from cranial mechanisms in order to study this phenomenon was proposed by Courtney et al [8]. This is because in the previous models, even if the blast wave was focused on the thorax, it was not known how much of the blast pressure reached the brain via the thoracic region or through other

mechanisms. They recommended that a blast-like pressure wave be generated under water and transmitted to the thorax in an animal model. The cranium in the model would thus be blocked from receiving any impact from the pressure wave and the effects could then be isolated and studied.

Another effect of blast is the formation of a low-frequency electromagnetic field. The skull piezoelectricity then creates intense electromagnetic fields in the brain on the order of 10 V/m over pulses with a duration of a millisecond, which are many times higher than the Institute of Electrical and Electronics Engineers (IEEE) safety standards and regulations [9]. This electromagnetic field may also be exacerbated by the mechanical blast injury. Measurements of shocked skull bone during blast experiments will need to be carried out in order to corroborate these predictions.

2.5 Ideal Blast Waves

There are many sources of blasts. Such sources produce a pressure wave in air by rapid energy release. Stored energy in a compressed gas or vapor can produce explosions. Some examples include the muzzle blasts from a gun and the failure of high-pressure gas storage vessels. Explosion sources also occur during the rapid vaporization of a thin metal film or fine wires. More well-known blast sources are from chemical or nuclear reactions, and the sudden increase in air pressure causes a shock wave to form. This shock front is almost instantaneous, and causes nearly discontinuous increases in temperature, density, and pressure. This blast wave transmits through the air in a nonlinear manner [10].

Several equations have been proposed to model the shape of blast waves. Flynn assumed linear pressure decay while considering the blast loading of structures. The linear relation is given by the following equation [11]:

$$P(t) = P_0 + P_s\left(1 - \frac{t}{t^*}\right) \tag{1.1}$$

where *P(t)* is the overpressure at a fixed location, the peak overpressure right behind the primary shock is P_s, t is the time interval after the primary shock arrival, and t^* is the positive duration, or the time when the pressure first crosses the horizontal axis. This form is oversimplified, and Ethridge demonstrated an equation which fits many gage records over most of the positive phase of the blast using the following relation:

$$P(t) = P_0 + P_s e^{-ct} \tag{1.2}$$

where c is some constant [12]. A pressure wave can also be approximated using the Friedlander equation, which can be used to describe the physical properties of an ideal blast shock wave. This equation is used in various studies, including [13]. The Friedlander equation is as follows [14]:

$$P = P_s e^{-\frac{t}{t^*}}\left(1 - \frac{t}{t^*}\right) . \tag{1.3}$$

An example of a Friedlander blast wave is given in Figure 2.3.

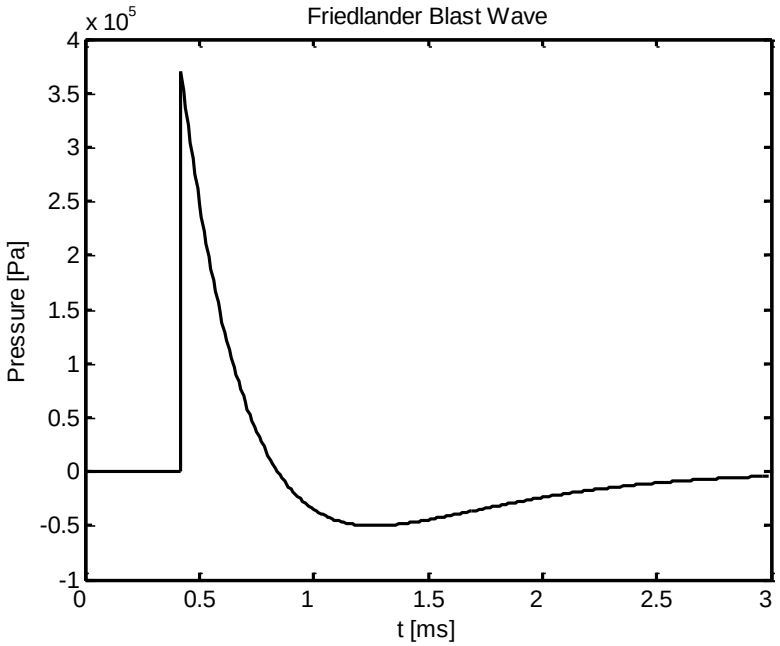

Figure 2.3: Friedlander Blast Wave.

ConWep is a collection of conventional weapons effects calculations and includes air blast routines, breach, cratering, ground shock, and fragment and projectile penetrations. The air blast data used comes from a series of experiments carried out by Kingerly and Bulmarsh [15]. These experiments were carried out in the 1980's. The ideal blast wave equations have been derived using such data, and serve as best-fit estimates.

2.6 Blast Wave Simulations

Shock wave propagation has been modeled using molecular dynamics (MD) and finite element methods; however, this limits the model to a single scale of physics, on an atomistic scale and on a continuum mechanics scale respectively. A non-equilibrium multiscale dynamics method has been created to simulate the non-equilibrium thermal-mechanical coupling processes during shock blast wave propagation at small scales [16]. Computer simulations through the use of finite element analysis have also been performed to model the effectiveness of helmets in preventing and diminishing the effects of shrapnel and blast impacts [17]. Ganpule et al. specifically used finite element discretization on material models to understand the physics of blast shock wave flow past both the helmeted and non-helmeted human head to specifically understand what part geometry plays on the mechanics of the flow [18]. They performed an analysis on Lagrangian bodies (head, helmet, upper body models) immersed in an Eulerian domain (air). From this study, they were able to determine the effects of a shock wave on an unprotected head, a head with a helmet with varying head and helmet gaps, and a head protected by a helmet with tightly fitting foam pads.

2.7 Experimental Studies of Traumatic Brain Injury

Several studies have been conducted that demonstrate that the skull does very little to absorb the blast pressure caused by explosions. These tests have been performed both on animals

and human head models [19-21]. In one such study, a swine head model using linear elastic material properties demonstrated that the undiminished pressure waves travelled through the skull to impact the brain [21]. The air overpressure was a primary cause of traumatic brain injury. Another example included a rat head being subjected to an overpressure wave with a time duration of 4.5 ms and a peak overpressure of 42 kPa and data was collected using pressure probes inside the rat's brain [19]. Zhang et al. used a head model consisting of a polycarbonate transparent skull with tissue of additive Sylgard 527 gel [20]. In this test, there was very little strain observed in the brain material. The cause of the brain trauma observed was caused by a pressure-driven injury mechanism from the air pressure increase. Such tests are useful for computer simulations of traumatic brain injury because the data contained therein can be used for computational model validation and calibration in order to achieve accurate simulations of blast impacts.

2.8 Numerical Simulations of Traumatic Brain Injury

Various models have been created to simulate blast waves impacting a human head. A finite element mesh was initially created that could be parameterized to allow for various head sizes [22]. This gives the ability to observe the effects of blast waves impacting the head of a child, woman, or man, along with the simulation of varying head sizes between each group. Grujicic et al. demonstrated the use of a Lagrangian-domain model for a human head to simulate blast-induced traumatic brain injury. They obtained results for pressure and stress measured at different points in the head model. Their results contained discrepancies in the TBI threshold established from documented cases of head-to-head collisions, which was attributed to material models used that did not accurately take into account micro-anatomic aspects of tissues and cells inside the skull [23].

Experimental tests often demonstrate the need of helmets which can absorb blast pressure and thus mitigate the effects of blast impact on the human brain. At the same time, these helmets must protect the head from blunt trauma caused by shrapnel-induced wounds. Ganpule et al. performed a finite element analysis on the role of the helmet in mitigating blast shock wave propagation. They concluded that the highest reflected overpressure when a shock wave impacts a human head are the regions of concavity, especially at the nasion, which is the nose-eye cavity. Other areas of concavity include the nose tip and forehead. The curvature of the helmet and head is another important factor because it governs the flow field. Gaps between the helmet and the head also created a nonlinear increase in overpressure and impulse on the other side of the head, with the maximum overpressure occurring about 140° from the direction of the blast wave. However, these large overpressures are lower than those experienced at the oncoming blast wave side of an unprotected head. To eliminate the overpressure and impulse increases when a helmet is worn and to provide the best protection against blast wave impacts, tight foam pads were used between the helmet and head to prevent pressurization in the gap between the helmet and head [18].

Kulkarni et al. carried out a comparative study on ballistic helmets [2]. This review included current helmet materials such as Kevlar® K29, K129 fibers, and thermoset resins, and possible future materials to be used for helmets, such as thermoplastic polymers and nano-composites. They considered several constitutive models for brain tissues and discussed the effectiveness of current helmets in preventing traumatic brain injury.

The helmet analysis included the use of several material properties for the helmet in order to model the effectiveness of such materials in mitigating the effects of blast wave impact on the human head. It was concluded that lateral explosions cause higher pressures and shear stresses

than a frontal explosion [24]; and helmets do not cover the face, and therefor allow the transmission of waves into the intra cranial cavity.

2.9 Analytical Model Creation

The creation of the computational models are usually carried out using MRI data to create STereoLithography (.stl) files to perform 3D finite element simulations [25]. Following the creation of the geometric model, tetrahedral or hexahedral meshing algorithms can be implemented to generate the equivalent finite element mesh.

Another model creation method is voxel meshing, where the surface detection and mesh creation stages are combined in one process. Keyak et al. created an automated method of using computed tomographic (CT) scan data to derive bone geometry and then create a patient-specific 3D finite element model [26]. This method created finite element models of human femur bones. In voxel meshing, the volumetric pixels (voxels) are separated using segmentation techniques. These separated regions are exported as hexahedral elements, and conformity of the mesh at interfaces is assured. Chen and Ostoja-Starzewski created a human head model with five layers, the scalp, skull, cerebral spinal fluid, gray matter, and white matter using voxel meshing [27]. They validated their finite element model using a previous cadaver experiment of frontal impact. Others have also used voxel meshing to create finite element models, such as Taylor and Ford in their simulation of blast-induced traumatic brain injury [28].

There are several commercial software packages available to create finite element meshes. These include Mimics, Simpleware, Scan23D, and Amira. Free software can also be used to create these finite element meshes, although at an expense of time and effort. Some of the programs include ITK Snap, MeshLab, NetGen, and ReMesh.

2.10 Material Properties

The model of the head is incomplete without the addition of the material properties of the brain, cerebral spinal fluid, and skull. These properties can be somewhat difficult to obtain, especially the viscoelastic properties of brain tissue and cerebral spinal fluid. There have been several methods devised to measure the mechanical characteristics of the cerebellum. An early method used unconfined compressive loading to model the viscoelastic properties of brain tissue. This data was used in a finite element simulation of an unconfined compression experiment [29]. There are several limitations to this method, including the prevalence of non-compressive forces in ballistic and shock wave impacts. One study measured the viscoelastic properties of the cerebellum and cerebrum using Magnetic Resonance Elastography (MRE) [30]. This method enables the collection of data without invasive surgery or the need to perform tests on cadavers. Another model demonstrated the addition of tension properties and was able to model brain tissue in compression and extension [31]. A non-linear viscoelastic material model for brain tissue was developed in a corresponding FE model to create a manner for simulating traumatic brain injury caused by shrapnel or other mechanical insult on the head [32]. Zhang et al investigated temporary cavities and pressures in order to create a better study of ballistic head injury [33]. Another result was that the brain material shows non-isotropic behavior [34, 35]. Several models have been used to describe the material properties of the brain and cerebral spinal fluid in the past. As shown below, there are several methods for characterizing the material properties of the brain. In order to achieve accuracy in a shock blast simulation, the model for the brain material must represent different mechanical behaviors and load responses in a single framework and must be valid for large strain rates at high strains. The skull is normally characterized by a linear elastic model.

2.10.1 Linear viscoelastic models

Linear viscoelastic models can be used to model tissue responses, such as that used by Nicolle, et al. to describe creep and relaxation responses in the human brain [36]. Viscoelastic models are frequently used to model tissue responses to mechanical forces. However, these are only suited to situations where there is small strain, and are not useful in describing the responses of brain tissue when exposed to blast wave impacts.

2.10.2 Large strain hyper-elastic models

Another model commonly used in biomechanics is a large strain hyper-elastic model. Velardi et. al. used polynomial strain energy functions to describe material responses [37]. There are several parameters used in the polynomial functions, and experimental and numerical results demonstrated the sensitivity of such a model to the test direction. Another example of the use of the large strain hyper-elastic model is given by Wright et al. [38].

This model is inadequate for traumatic brain injury due to blast waves because the strain energy density function depends on the fourth invariant of the Cauchy-Green strain tensor, which is unable to accurately predict the behavior of the human brain at medium to high strains and shear loading. Once again, the high strains expected during blast shock waves are not adequately predicted using the large strain hyper-elastic models.

2.10.3 Large strain hyper-viscoelastic models

Large strain hyper-viscoelastic models are used to more accurately characterize the tension/compression and shear behavior of the human brain by combining the methodologies of hyper-elasticity and linear viscoelasticity. The most commonly used constitutive equations for modeling the quasi-static response of the human brain are the Mooney-Rivlin hyper-elastic

model and the Neo-Hookean material model. Chafi et al. [39] used the Mooney-Rivlin hyper-elastic model to represent constitutive material properties of the human brain. Another model was proposed by Darvish and Crandall, where they compared two nonlinear constitutive models, a third-order non-linear Green-Rivlin viscoelastic model and a third-order quasi-linear viscoelastic model. The Green-Rivlin model demonstrated superiority at high frequencies, and worked for any shear strain range [40]. There are several other variations of these models which have been proposed, each capturing different aspects of the actual material properties of the human brain.

2.10.4 Helmet Properties

The properties of the helmet and foam pads also need to be considered. Helmets were worn throughout the middle ages by the Sumerians, Greeks, Romans, and Assyrians. The first modern steel combat helmet was the French Adrian helmet during World War I. The United States developed the steel Hadfield helmet shortly after. The steel helmet was improved in the early 1960s by using Kevlar® fibers. More modern helmets have also been developed, including the Advanced Combat Helmet (ACH) and the lightweight helmet (LWH) used by the United States Marines [2]. Several materials have been used or proposed for use in helmets of the future. These materials include Nylon 66, Kevlar® K129, carbon nanotubes, E-glass reinforced polyester, and ultra-high molecular weight polyethylene (UHMWPE). The padding is usually made of foam, which can be modeled using a non-linear viscoelastic formulation [41] or a linear elastic model. The helmet materials are typically modeled using the linear elastic properties such as Young's modulus and Poisson's ratio.

2.11 Related Studies of Blast Impact on Steel Plates

A study on the performance of mild steel perforated plates to mitigate blast waves demonstrated that the perforated plates with small hole sizes reduced damage by mid-point deflection and increasing the tearing threshold impulse [42]. This may be useful in the design of helmets; however, problems could arise with lowering the ability of the helmet to protect against shrapnel impacts especially with small holes. Perhaps a honeycomb-like structure would be beneficial. Schimizze, et al. [43] performed an experimental and numerical study of blast induced shock wave mitigation in sandwich structures using a wide variety of materials and material properties. They demonstrated the importance of density and acoustic impedance mismatch, as well as the importance of porosity to mitigating the effects of air blasts [43].

Another experimental result was obtained by Wu and Sheikh. The pressure blast wave was obtained experimentally and deflections were compared to a finite element model [44]. This type of comparison can be used to ensure that the plate blast simulation performed in Abaqus is similar to actual experimental results.

Neuberger et. al. studied the dynamic response of clamped circular plates to close-range and large blast loadings [45]. Their study focused on the accuracy of using scaled-down experiments to predict what would happen in a full-scale spherical blast. They also demonstrated the use of various models for describing the material properties of steel, including the Johnson-Cook model and a bilinear model.

2.12 Conclusions

In this chapter, the relevant literature highlighting the various tasks involved in the understanding of blast induced traumatic brain injury is studied. This review provides insight into the limitations of the current techniques in understanding the effects of blast waves and their

interactions with the human head and development of possible remedial measures using helmet protection systems.

CHAPTER 3 – COMPUTATIONAL PROCEDURE

3.1 Abstract

The major part of this chapter is devoted to the discussion of various methodologies that were identified during the literature study highlighted in the previous chapter on blast impact mitigation and its studies on blast induced human traumatic brain injury. The major aspects in simulating the blast impact and mitigation studies are highlighted. It also describes some of the important concepts used in modeling the blast and creating a head-helmet model. These include the representation of blast waves using Friedlander-type equations for estimating blast impact incident pressure, the Mooney-Rivlin hyperelastic models for simulating the properties of the brain tissue, and the use of micromechanical methods for estimating the properties of porous structures within the human head. There have been various methods devised to simulate blast traumatic brain injury. The methods proposed for the current computation is an amalgam of different methods performed by others and combined in a unique way, with several other innovative factors added.

3.2 Blast Impact Experiments

Several experiments have been performed in the past to simulate blast impacts, resulting in a plethora of experimental data. In this work, data collected from air blasts caused by actual explosions has been used, as opposed to data collected using shock tubes. Such an approach provides a more realistic model of what occurs during blast shock wave impact and the subsequent development of blast-induced traumatic brain injury.

3.3 Blast Shock Wave Simulations

One of the most efficient means of representing a blast impact is the use of ConWep based data. ConWep is a collection of conventional weapons effects calculations and includes air blast routines, breach, cratering, ground shock, and fragment and projectile penetrations. The air blast data comes from a series of experiments carried out by Kingerly and Bulmarsh [15]. Abaqus is a finite element (FE) analysis software. The CONWEP charge property parameter is used in this program, which simulates an explosion in air based on the empirical data used to create the ConWep calculations, and creates a time history of pressure loading. To use this parameter, data must be entered to define the charge properties. This data includes the equivalent mass of TNT in any mass unit, a multiplication factor to convert from that mass unit to kilograms, and multiplication factors to convert from the analysis length, time, or pressure to meter, second, or Pascal (Pa). A reference point is selected for the location of the initial TNT blast, and a surface is selected for interaction with the incident blast. The software does not currently recognize objects overshadowing a surface which may be impacted by the blast. The parameters used in this work include 3 different magnitudes of blast waves impacting the human head from 0.038 kg TNT, 0.093 kg TNT, and 0.227 kg TNT at a distance of 0.8 m. All scaling factors are kept at 1 since the simulations are accomplished on a full-scale model.

Several researchers have used ConWep to model the response to blast loads. Blanc et al. demonstrated the use of ConWep loading in modeling the response of structures to blast loads [46]. They compared a Lagrangian ConWep simulation to a Lagrangian-Eulerian coupling. They determined that the Lagrangian approach was more precise because it simulated the Mach wave front and a perfect ground reflection, and reflected pressures better. It tended to allow for a smaller model since the surrounding air does not need to be modeled, just the structure being

impacted. Another group used ConWep simulations to estimate the amount of explosives and ammunition that could be safely stored in a given location [47]. The results obtained match those obtained by more complex hydrodynamic computations and serve as a means to simplify the problem. The simplicity and usefulness of the ConWep simulations is why they were chosen for this work to simulate the impact of a blast wave on the human head.

3.4 Modeling of Human Head for Traumatic Brain Impact Measurement

This work is focused on the effects of blast-induced traumatic brain injury, as opposed to traumatic brain injury which occurs from sporting injuries, automotive accidents, work-related accidents, or other events. The finite element analysis software Abaqus is used to perform the simulations of blast shock wave impacting a human head. In this study the head model was created and constrained at the base of the neck to simulate an attachment to a human torso. The role of the helmet in protecting the brain from direct shock pressure waves is first studied and then compared with an unprotected head, and the potential for a visor in protecting from the effects of blast waves is left as a study for a future work.

3.5 Numerical Simulations of Traumatic Brain Injury

This study partially follows the process outlined by Vonach et al for creating the model of the human head [25]. The model created can be used to perform simulations of shrapnel and blast wave traumatic brain injury. The finite element model of the human head was obtained from the MRI data obtained from the Visible Human Female database from the National Library of Medicine [48]. The MR/CT images were converted to a FE mesh at multiple stages using various software programs. This model was then simulated using Abaqus to perform finite element analysis to study the effects of blast induced pressure differences in the human head with and without the aid of a helmet.

3.5.1 Human Head Model Creation

The first step in performing a multiscale analysis of blast or shrapnel impact on a human head is the creation of a valid finite element model. Digital Imaging and Communications in Medicine (DICOM) imaging was obtained online from Computed Tomography (CT) scan data available for medical referencing from the Visible Human Female database.

ITK Snap is a free software application used to segment 3D medical images. The images were combined and manual segmentation was performed on the images to create a 3D STereoLithography (.stl) file of the human skull, cerebral spinal fluid, and brain. This process involved tracing the outlines of the skull and cerebral spinal fluid manually on a series of 234 DICOM images of a human head. Figure 3.1 demonstrates the tracing procedure executed on the DICOM files.

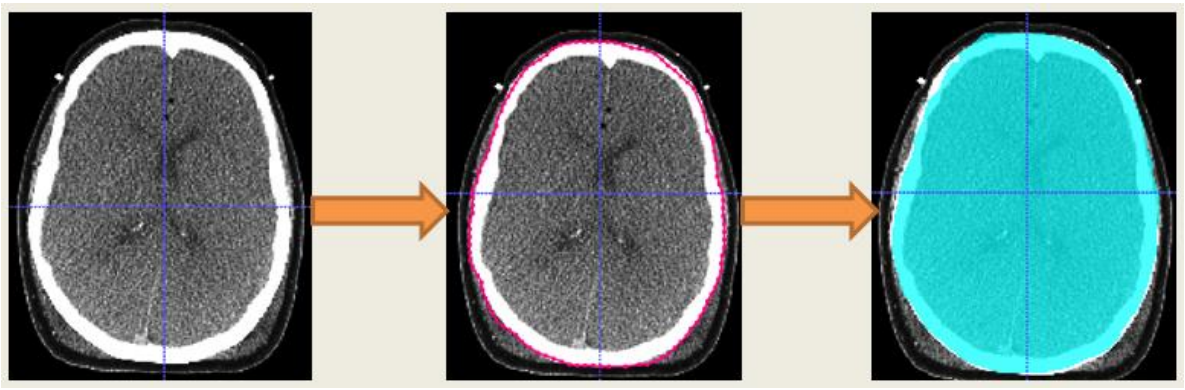

Figure 3.1: Steps of creating a skull model.

Because this process was performed manually, the resulting .stl files are not smooth. From the stepped .stl file, various methods were used to create a smooth .stl file to be used for the FE model generation. MeshLab is a free software program which enables the processing and editing of 3D triangular models. Once the images were analyzed for “manifoldness”, the Poisson surface reconstruction filter, followed by Laplacian smooth filter, and other filters were applied to create a smooth .stl file for the skull and cerebral spinal fluid. Because of the difficulty in

manually segmenting the DICOM imaging data for the cerebral spinal fluid, MeshLab was also used to create a model of the brain by decreasing the cerebral spinal fluid .stl file by a certain scaling factor. A more rigorous model of the cerebral spinal fluid may be created from more detailed MRI or CT scan data. The current model serves as a good approximation of the human skull, cerebral spinal fluid, and the brain.

In order to obtain a mesh which is valid for FE simulations in Abaqus, the .stl file also needed to be cleaned up using a program called ReMESH. ReMESH is a free program which is used to edit and repair triangle 3D files. It was used on the brain, skull, and cerebral spinal fluid .stl files to check the geometry of the models. The models were checked to make sure that there were no more problems with spurious triangles or holes in the .stl file; as such errors prevent the creation of a valid finite element mesh. The "Check Geometry" function checks for holes, degenerate (zero-volume) triangles, and overlapping triangles. The holes can be filled manually using a fill holes interaction, and many degenerate and overlapping triangles can be removed using the "Remove Degenerate Triangles" and "Remove Overlapping Triangles" commands using the option "Check and Repair." This software enabled the ability to zoom in and check the problem triangles and create a valid model. It also has algorithms to resample the model, which makes it smaller and easier to simulate. This process was performed on the .stl files of the brain, cerebral spinal fluid, and skull. It also has a Laplacian Smooth algorithm which was used to make the 3D models smooth. This program, combined with the abilities of MeshLab, enabled a smooth and accurate model of the brain, cerebral spinal fluid, and skull as shown in Figure 3.2.

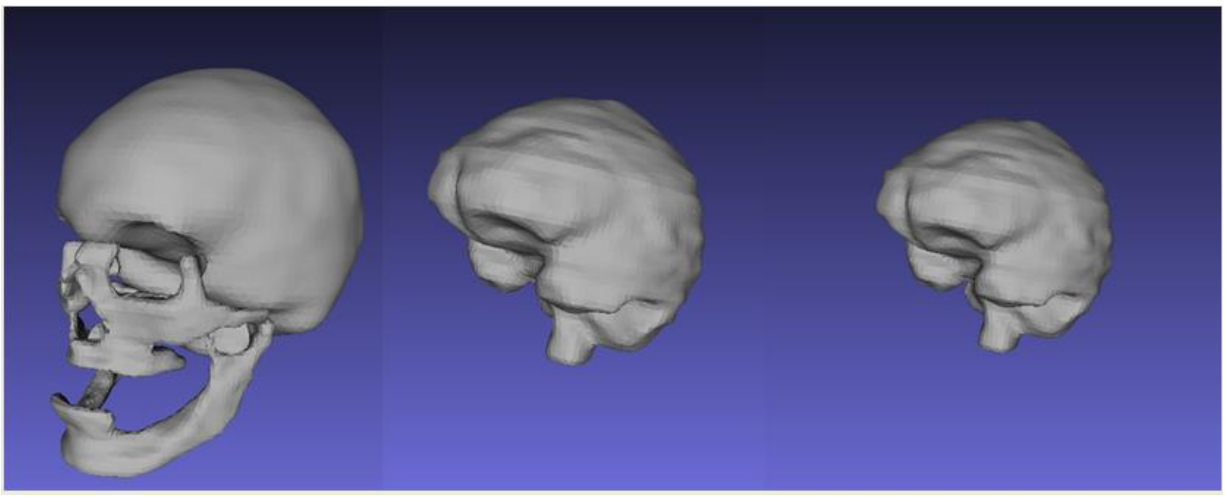

Figure 3.2: Final smoothened .stl models of the skull, cerebral spinal fluid (CSF), and brain.

3.5.2 Finite Element Mesh Creation

The three files produced were all solid models of the head, cerebral spinal fluid, and brain. Trelis is software which is a pre-processor for FE analysis and other applications. It is used to create meshes and modify .stl files containing 3D models. The command 'set developer commands on' was used to allow the use of the volume Boolean function to subtract the cerebral spinal fluid from the skull and the brain from the cerebral spinal fluid. This provided hollow, real-life models of the skull and cerebral spinal fluid. The mesh which was then used in Abaqus was created using the command 'mesh volume all from facets'. This produced a volume and surface mesh for the different layers which was a tetrahedral mesh, since the elements of .stl files are comprised of triangles. Figure 3.3 demonstrates the steps of the model and finite element mesh creation.

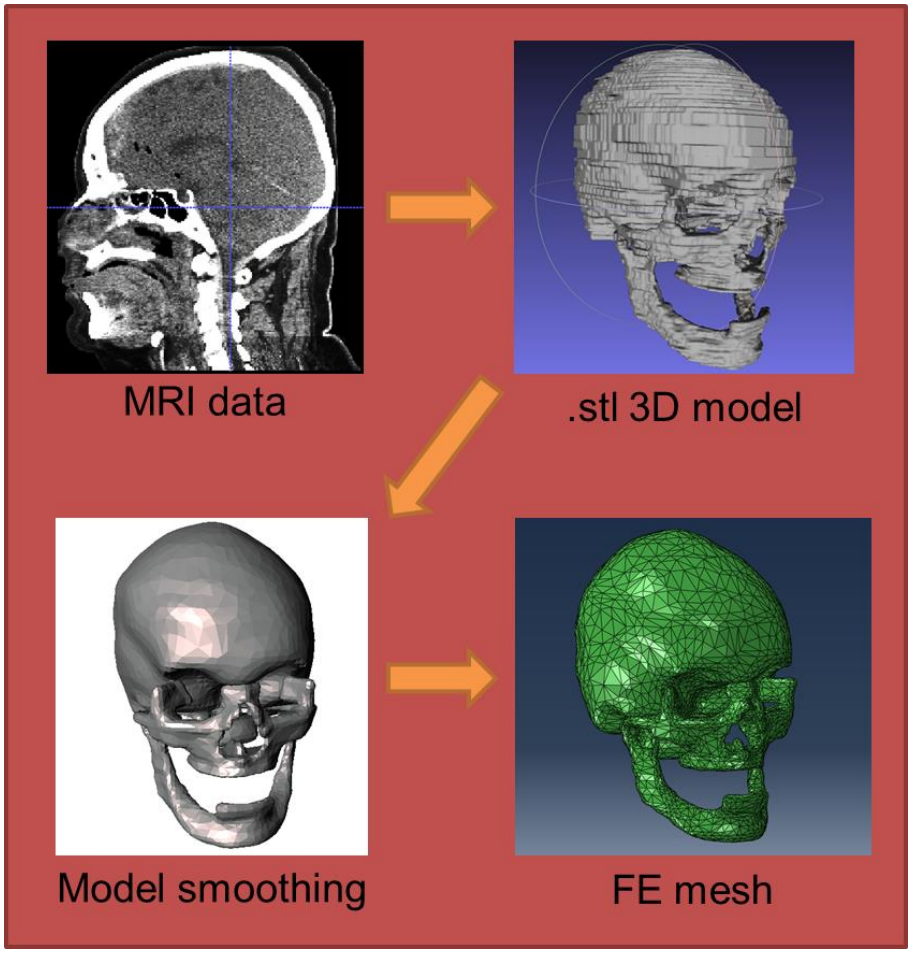

Figure 3.3: Head model and mesh creation.

3.5.3 Finite Element Simulation

The objective of the finite element simulations in this study was to apply CONWEP blast loading and compare computational results obtained from this blast loading simulation to experimental results. The analysis were performed in Abaqus using a dynamic explicit finite element analysis with blast loading simulations on the model human head developed from the MRI/CT images as described earlier. The FE geometry of the human head model includes a brain, surrounding cerebral spinal fluid, and a skull. The head is fixed at the base of the neck with encastre boundary conditions, meaning there are no translations or rotations allowed in any

direction (U1 = U2 = U3 = UR1 = UR2 = UR3 = 0). This simulates the addition of a torso attached to the neck.

The head model contains 6092 nodes total. The skull model contains 5998 elements, the cerebral spinal fluid model contains 5352 elements, and the brain model contains 6745 elements, for a model total of 18095 elements in the model of the head. All of the elements are type C3D4, meaning 4-node linear tetrahedrons. The encastre boundary conditions as well as the explosion source are indicated in Figure 3.4.

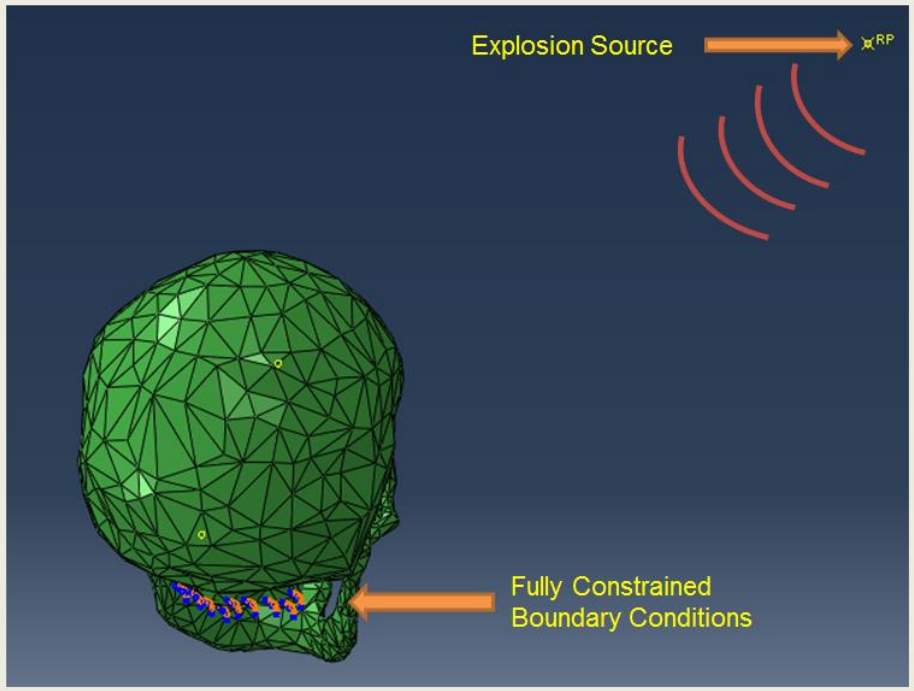

Figure 3.4: Boundary conditions and explosion source.

3.5.4 Helmet

The primary function of helmets is to absorb ballistic impacts from shrapnel or bullet strikes. Nguyen performed a series of analytical and FE experiments on the effects of curvature on stresses in curved beams [49]. He discovered that as the radius of curvature increases, the radial stress decreases. Tham et al. studied the effects of curvature on ballistic helmets by

creating a detailed FE model of a Kevlar® helmet [50]. The created model accurately simulated the ballistic test standards for Kevlar® 29 helmets.

A crude helmet was constructed using Abaqus and Trelis. The design of the helmet incorporated the use of splines to conform to the shape of the human head model already created. The helmet contains an inner layer of padding. These items were also meshed in Trelis. The helmet contains 1564 elements and the inner padding contains 1668 elements. These are C3D4 tetrahedral elements.

3.6 Material Properties of Soft Tissues

3.6.1 Brain Material

In this study the heterogeneity of the brain material and its non-isotropic behavior is not taken into account in the study of traumatic brain injury and is left as a subject for future work. In this study a model similar to that used by Chafi et al. [39] is used to model the hyper-elastic material properties of the human brain called the Mooney-Rivlin model for large strain hyper-viscoelastic materials. The strain energy function for the Mooney-Rivlin model is defined as:

$$W = C_{10}(J_1 - 3) + C_{01}(J_2 - 3) + \frac{1}{D_1}(J_{el} - 1)^2 \tag{2.1}$$

where W is the strain energy potential, J_{el} is the elastic volume ratio, J_1 is the first invariant of the deviatoric strain, J_2 is the second invariant of the deviatoric strain, and C_{10}, C_{01}, and D_1 are material constants dependent on temperature. Linear viscoelasticity is used to estimate the second Piola-Kirchhoff stress by the following convolution integral:

$$S_{ij} = \int_0^t G_{ijkl}(t - \tau)\frac{\delta E_{kl}}{\delta \tau} d\tau \tag{2.2}$$

where S_{ij} is the second Piola-Kirchhoff stress, $G_{ijkl}(t-\tau)$ is the relaxation modulus function for the different stress measures, and E_{kl} is the Green's strain tensor. To compute the Cauchy stress associated with this, the following equation is used:

$$\sigma_{ij} = JF_{ij}^{T} \cdot S_{km} \cdot F_{mj} \tag{2.3}$$

where the Cauchy stress is σ_{ij}, F is the deformation gradient tensor, and J is the Jacobian of transformation. Finally, this stress is superimposed to the stress tensor which was determined from the strain energy function. A Prony series can be used to represent the relaxation modulus for an isotropic material as follows:

$$G(t) = G_0 + \sum_{i=1}^{n} G_i e^{-\beta_i t} \tag{2.4}$$

where β_i is the decay constant and G_i is the relaxation modulus. The parameters selected for the brain are a density of 1040 kg/m^3 [41] with Mooney-Rivlin coefficients C_{10} = 3102.5 Pa, C_{01} = 3447.2 Pa, and D_1 = 1.095 GPa from a bulk modulus of 2.19 GPa [39].

3.6.2 Cerebral Spinal Fluid Material

The cerebral spinal fluid is modeled using fluid-like properties. The final Hugoniot pressure is used as the constitutive relationship. In this relationship, $\dot{p} = -K\dot{\varepsilon}_{ij}$, where K is the bulk modulus of elasticity, $\dot{p}$ is the pressure rate, and $\dot{\varepsilon}_{ij}$ is the deviatoric strain rate [39]. This material property is considered using the linear $U_s - U_p$ equation of state (EOS). The linear form is

$$p = \frac{\rho_0 c_0^2 \eta}{(1-s\eta)^2}\left(1-\frac{\Gamma_0 \eta}{2}\right) + \Gamma_0 \rho_0 E_m \ . \tag{2.5}$$

The linear response described here is given by setting the parameters s = 0.0 and Γ_0 =0.0 since $K = \rho_0 c_0^2$ [51]. This gives a c_0 of 1451.127 m/s using a bulk modulus of 2.19 GPa [39]. The density is taken as 1000 kg/m^3.

3.7 Material Properties of Hard Tissues

3.7.1 Skull Material

Micromechanics is the analysis of composite materials at a constitutive level. Mechanical properties may be estimated using various micromechanics models and compared to results obtained experimentally. Although these methods do not match exactly the results obtained experimentally, they provide a good model and method of analysis to describe appropriate composite behavior by means of mathematical homogenization. In a mathematical homogenization, the heterogeneous composite material is replaced by an equivalent homogeneous continuum using a suitable homogenization technique. The homogeneous continuum is based on a statistically equivalent homogeneous volume element, called the representative volume element (RVE) which represents the material in the lower order - the microscale and collectively represents the global structure. One such method is the Reuss bound. It is the lower bound to the methods of predicting properties of composite materials because it assumes that the stress is everywhere uniform throughout the composite material [52]. The Young's modulus may be calculated using the Reuss bound by the following equation:

$$E_c = \left(\frac{f}{E_f} + \frac{1-f}{E_m} \right)^{-1} \tag{2.6}$$

Where f is the volume fraction of the fiber, E_f is the Young's modulus of the fiber, and E_m is the Young's modulus of the matrix.

Alternately, the Voigt bound predicts properties of composite materials assuming that the strain is everywhere uniform [53]. It embodies the upper bound to the method of predicting these composite material properties. The Young's modulus may be calculated using the Voigt bound by the following equation:

$$E_c = fE_f + (1-f)E_m \tag{2.7}$$

The Voigt and Reuss bounds demonstrate what is known as the Rule of Mixtures, and represent an upper and lower bound for the properties which may be simulated using micromechanics. Let us consider a representative volume element (RVE) of an infinite homogenous matrix embedded with a dilute inclusion and subjected to a homogenous displacement boundary condition and producing a uniform strain ε_{ij}^{o}. Eshelby has shown that under the above conditions, the ellipsoidal inclusion experiences a uniform eigenstrain ε_{ij}^{*} [54, 55]. By applying the eigenstrain method, the effective modulus of the RVE can be calculated and the Mori-Tanaka (MT) method is used in this work. The MT method treats the different inclusions as distinct regions and does not take into consideration the geometry [54, 55]. To elucidate the expressions for the MT method, we assume that the composite is composed of k phases. The stiffness of the matrix is denoted by C_m and the volume fraction of the matrix is denoted by v_m. The kth phase (or inclusion) has a stiffness of C_k and volume fraction of v_k. The dilute strain concentration factor for the kth phase, denoted by A_k^{dil}, relates the volume averaged strain in the kth inclusion to that of the matrix [54, 55] and it is obtained from,

$$\left[S_k + C_m\left[C_k - C_m\right]^{-1}\right]A_k^{dil} - \sum_{n}^{K-1} v_n S_n A_n^{dil} = -\mathrm{I} \tag{2.8}$$

where $(k,n)=\{f,g,...K-1\}$, and S_k is the Eshelby Tensor for the dispersed inclusions. The effective modulus of the composite (i.e., matrix with inclusions), C, is found from [56].

$$C = C_m\left[\mathrm{I} - \sum_{k=1}^{K-1} v_k A_k^{dil}\right] \tag{2.9}$$

The skull is modeled as a linear elastic model. In order to perform a multiscale approach to the simulation of traumatic brain injury from blast impacts, a Mori-Tanaka(M-T) [57] based homogenization of the porous bone structure is performed. The M-T method falls between the Voigt and Reuss bounds in homogenizing composite materials. Skull bone can be viewed as a composite material. Composite materials consist of a particle phase and a matrix phase. This simulation uses a porosity of 0.82, which is that of a cancellous bone, a Poisson's ratio of 0.32, and Young's modulus of 22 GPa [58] for the matrix material. The density of the skull is taken as 1412 kg/m^3 [41]. Linearly elastic and isotropic solids assumption can be made for the voids (pores) and matrix of the skull bone tissue [59]. The effective Young's modulus and Poisson's ratio of the composite bone tissue may be estimated using the Mori-Tanaka method using the following method [60]:

$$\bar{E} = 2\bar{\mu}\left[1+\frac{3\bar{K}-2\bar{\mu}}{2(3\bar{K}+\bar{\mu})}\right] \tag{2.10}$$

where

$$\bar{K} = K_0\left\{1+\frac{c(K_1-K_0)}{K_0+3\gamma_0(1-c)(K_1-K_0)}\right\} \tag{2.11}$$

$$\bar{\mu} = \mu_0\left\{1+\frac{c(\mu_1-\mu_0)}{\mu_0+2\delta_0(1-c)(\mu_1-\mu_0)}\right\} \tag{2.12}$$

and, $\gamma_0 = \frac{1+V_0}{9(1-V_0)}$; $\delta_0 = \frac{4-5V_0}{15(1-V_0)}$; $K_n = \frac{E_n}{3(1-2\nu_n)}, \mathrm{n}=0,1$ and $\mu_n = \frac{E_n}{2(1+\nu_n)}, n=0,1,$

$$\bar{\nu} = \frac{3\bar{K} - \bar{E}}{6\bar{K}} \ . \tag{2.13}$$

The homogenized modulus used in this study is taken as 2.174 GPa, with a Poisson's ratio of 0.253.

3.7.2 Helmet Material

The material properties for new and improved helmets are also computed using micromechanics and included in the shrapnel and blast wave tests. The Advanced Combat Helmet, which is a thermoset resin/Kevlar®K129 composite, has a tensile strength for the matrix of 7386 MPa and for the fiber of 3429 MPa. It has a tensile modulus of 195 GPa and 96 GPa for the matrix and fiber respectively [61]. The Advanced Combat Helmet has a density of 1440 kg/m^3, an effective Young's modulus of 1.24 GPa, and a Poisson's ratio of 0.36. The Enhanced Combat Helmet (EHC) is made of Dyneema® HB80 composite with an effective Young's modulus of 14.786 GPa, a density of 1157.2 kg/m^3, and a Poisson's ratio of 0.36. The padding can be taken to have a density of 136 kg/m^3, a Young's modulus of 8.0 MPa, and a Poisson's ratio of 0.2 [62].

3.8 Conclusion

This chapter was devoted to the discussion of various methodologies that were identified during the literature study highlighted in the previous chapter on blast impact mitigation and its studies on blast induced human traumatic brain injury. The major aspects in simulating the blast impact and mitigation studies were highlighted, and some of the important concepts used in modeling the blast and creating a head-helmet model were discussed. These included the representation of blast waves using Friedlander-type equations for estimating blast impact incident pressure using ConWep, the Mooney-Rivlin hyperelastic models for simulating the properties of the brain tissue, and the use of micromechanical methods for estimating the

properties of porous structures within the human head using the Mori-Tanaka method. The result is a working model for analytically computing the effects of explosion shock overpressures on causing bTBI.

CHAPTER 4 – ANALYTICAL SIMULATIONS AND RESULTS

4.1 Abstract

This chapter is divided into two main parts. The first part discusses a verification example to simulate the blast impact on a solid steel plate. The results obtained in this verification study are compared with experimental investigations in literature. Other materials are also incorporated into the plate model, to perform preliminary tests on novel materials that could perform better in mitigating blast shock wave impacts. In the second part, the human head model subjected to blast impacts is studied and comparisons are made between a head protected by a ballistic helmet and an unprotected head. The obtained results are also compared with literature. Further, the performance of new materials for the improvement of the helmet in mitigating blast shock wave impacts are also studied using the same model with different material properties.

4.2 Analysis of Solid Plate Under Blast Impact

RHA is a type of steel used in armored vehicles. Neuberger et al. performed a series of experiments to test the accuracy of scaling laws in performing scaled-down experiments of clamped circular plates subjected to large spherical blast loadings at close range. One such experiment was carried out on a circular plate with a diameter of 2 m and thickness of 0.05 m [45]. The blast originated at a distance of 326.6 mm, with a mass of 9 grams of PE4, which is equivalent to 11.7 grams of TNT [63]. In their study, Neuberger et al. performed experiments on metal plates as well as finite element analysis on the plate models. The finite element simulations were also compared with the experimental values. In the simulations they used several material

models to describe the stress experienced by the metal plate, including a bilinear model, the Johnson-Cook constitutive model, and a modified Johnson-Cook model which gave varying material properties depending on thickness [64]. Figure 4.1 indicates the experimental and finite element simulation of a detonation over a circular plate.

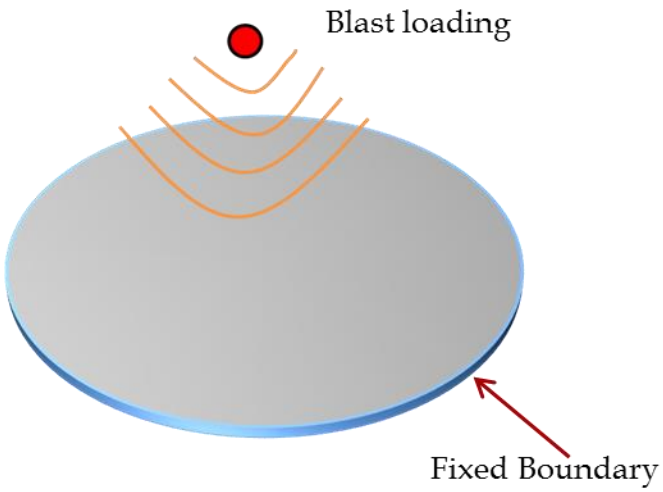

Figure 4.1: Blast loading of a circular plate.

The un-modified Johnson-Cook model for calculating stress was used to validate. The objective of the steel plate simulation performed here was to apply CONWEP blast loading and compare experimental and computational results. A finite element dynamic explicit analysis with blast loading simulations also provides a means to test new material properties and structures to better resist blast loads. The geometry of the analysis considered in the analysis is a solid plate following the dimensions described by Neuberger et al. [45]. Edges were fixed at all degrees of freedom, with the plate having a diameter of 2 m and a thickness of 0.05 m. The dynamic explicit analysis was performed for 4.5 milliseconds. The plate was discretized using 4821 C3D8R elements in Abaqus, having 3 layers of elements through the plate thickness. The detonation was simulated using CONWEP blast loading at a blast magnitude of 50 kg of TNT at a blast source 0.5 m from the center, and top surface of the plate.

4.3 Material Properties of the Steel Plate

Johnson and Cook created a constitutive model and data for metals subjected to high temperatures, large strains, and high strain rates. The von Mises stress is modeled using the following equation:

$$\sigma = [A + Bs^n][1 + C\ln s^*][1 - T^{(*m)}] \quad (3.1)$$

where ε is the equivalent plastic strain, $\dot{\varepsilon}^* = {\dot{\varepsilon}}/{\dot{\varepsilon}_o}$ is the dimensionless plastic strain rate for $\dot{\varepsilon}_o$ = 1.0 s^{-1}, T* is the homologous temperature, $[A + B\varepsilon^n]$ gives stress as a function of strain for $\dot{\varepsilon}^*$ = 1.0 and T* = 0, $[1 + Cln\dot{\varepsilon}^*]$ represents the effects of strain rate, and $[1 - T^{*m}]$ represents the effects of temperature [64]. The properties and coefficients used to simulate the material properties of the RHA steel plate are: density of 7850 kg/m^3, Young's modulus of 210 GPa, coefficient of expansion of 452 K^{-1}, Poisson's ratio of 0.28, A = 850 MPa, B = 355 MPa, C = 0.014, n = 0.26, m = 1, $\dot{\varepsilon}$ = 0.001 s^{-1}, transition temperature = 293 K, and melting temperature = 1800 K.

A convergence study was also carried out on the circular plate model. The results for normalized deflection (deflection/thickness) were found to be very similar to those obtained by Neuberger et al. A finer mesh with 18966 elements was created and the analysis was performed again. Figure 4.2 indicates the normalized deflection of the center of the steel plate. The results converge to the experimental values as the mesh gets finer. The maximum normalized deflection was approximately 1.92.

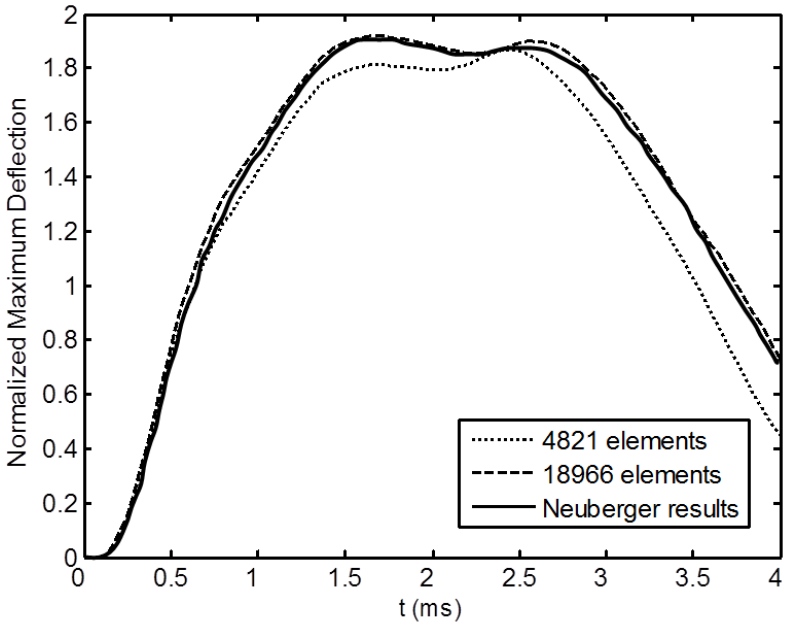

Figure 4.2: Comparison of normalized maximum deflection of steel plates demonstrating mesh convergence.

From the analysis, the maximum normalized stress was found to be 1.307. The normalized stress at the center and the stress distribution on the circular plate is indicated in Figures 4.3 and 4.4.

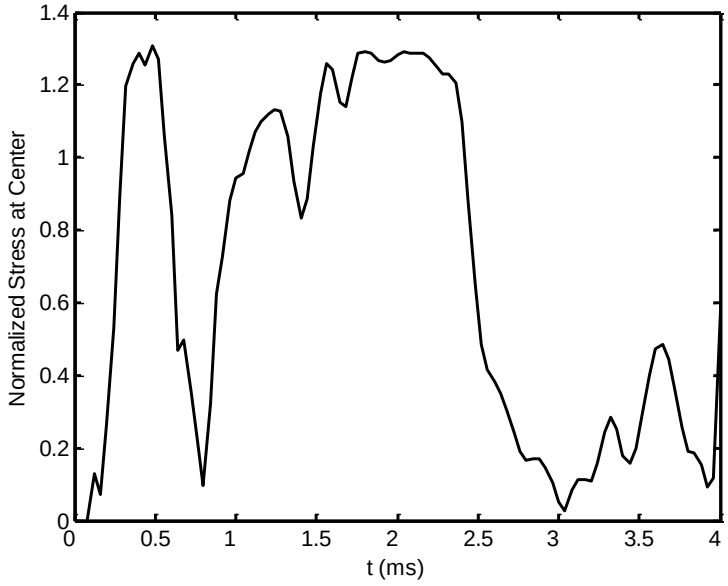

Figure 4.3: Normalized stress at center of circular steel plate.

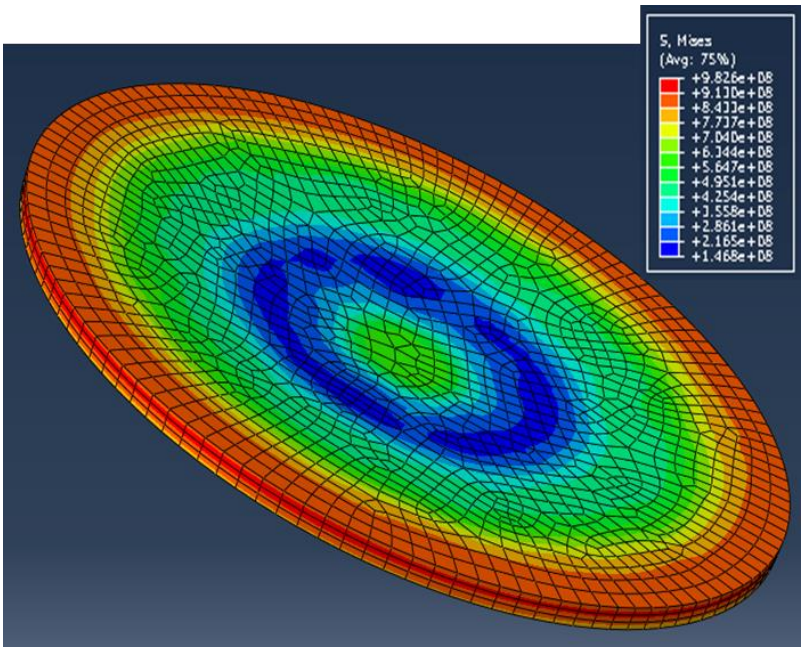

Figure 4.4: Stress distribution on the circular steel plate model.

4.4 Advanced Combat Helmet Material Properties Simulation

The next simulation demonstrates the effects of the same 50 kg of TNT at a distance of 500 mm on a plate of thermoset resin/Kevlar®K129 composite with a density of 1440 kg/m^3, an effective Young's modulus of 1.24 GPa, and a Poisson's ratio of 0.36 [62]. Realistically, a plate of 2 m diameter with a 0.05 m thickness made of this helmet material would not necessarily be very useful, however, the simulations obtained demonstrated the ability of this material to withstand pressure blasts and mitigate the effects of a blast wave. These results were then compared to those obtained using a new composite made as a combination of thermoset resin/Kevlar®K129 homogenized as a matrix and carbon nanotubes as the fibers in a new type of composite material.

4.5 New Helmet Material Properties Simulation

The new material proposed to advance the viability of military helmets in mitigating the effects of shock wave impact in causing blast-induced traumatic brain injury is a composite

material. The original composite material of the Advanced Combat Helmet is homogenized and treated as a matrix. Carbon nanotubes are treated as the fiber to provide additional strength and support in aiding the mitigation of shock waves impacting the human brain. The effective properties of the original ACH material are used, along with the properties of carbon nanotubes, a homogenized ACH material model based on the Mori-Tanaka homogenization schemes for fiber and matrix composite materials. Using LAMMPS, a molecular dynamics simulator, the Young's modulus of (5, 5) single-walled carbon nanotube was computed. The (5, 5) indices correspond to the number of unit vectors along 2 directions of a graphene lattice and correspond to a carbon nanotube diameter of 678 pm. The molecular dynamics simulation included a minimization of the input system, an equilibration to 300 K for 30000 steps, and a deformation test for 20000 steps at a strain rate of 0.01 ps^{-1}. Each time step was 0.2 fs and used the reactive potential function developed by Stuart et al. for the modeling of intermolecular interactions and chemical reactions in condensed-phase hydrocarbon systems [65]. The AIREBO potential function is used to model the carbon atoms of the carbon nanotube. Data obtained from the deformation was analyzed to provide the stresses required for a stress-strain plot. From the stress-strain plot, the Young's modulus was computed to be 1.004 TPa. The Young's modulus for a single-walled carbon nanotube obtained in literature is 1 TPa, with a Poisson's ratio of 0.14 [66] and a density of 1330 kg/m^3 [67]. A 5% volume fraction of carbon nanotubes was assumed in the analysis. The resulting composite had an effective Young's Modulus of 1.3772 GPa, an effective Poisson's ratio of 0.35522, with a density of 1434.5 kg/m^3. Figure 4.5 indicates a (5,5) carbon nanotube of length 5 nm.

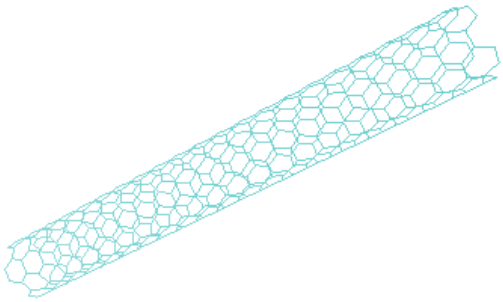

Figure 4.5: (5,5) carbon nanotube used to enhance helmet material.

Figure 4.6 demonstrates a comparison of the maximum principal stress at the center of the circular specimens. The carbon nanotube-enhanced material demonstrates a slightly higher peak value around 2.5 ms of 395.32 MPa, while the standard ACH material had a peak slightly later at 366.92 MPa.

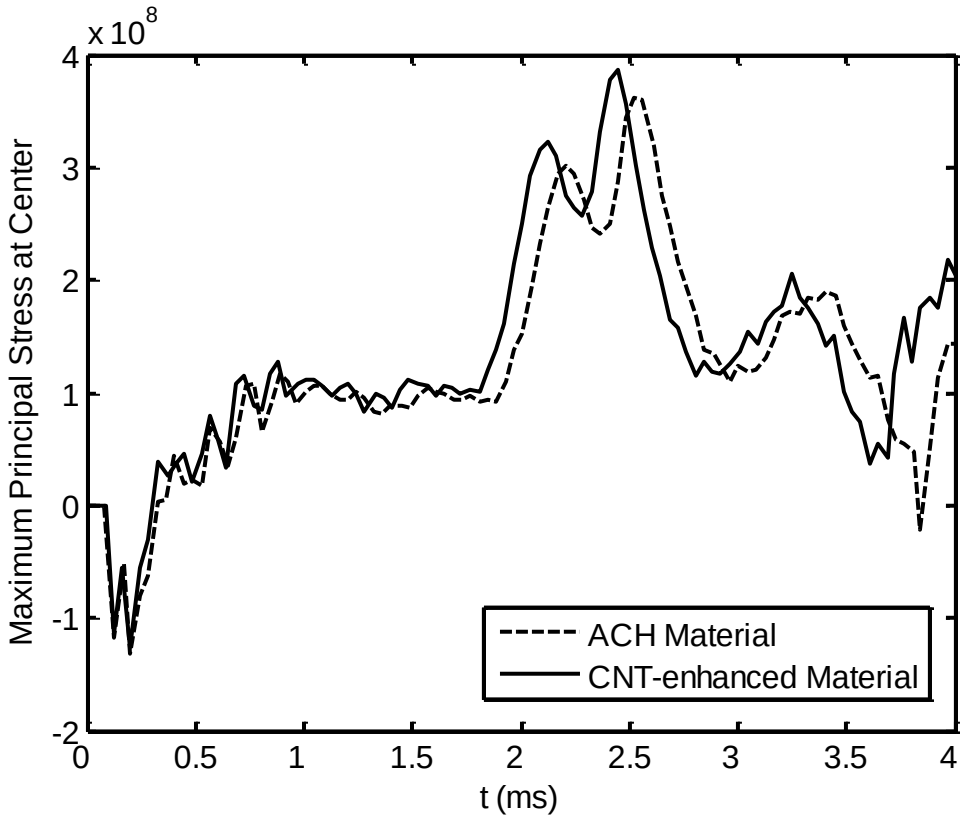

Figure 4.6: Comparison of maximum principal stress for two combat helmet materials.

4.6 Numerical Simulations on Human Head

Several simulations were then performed on two distinct models. The first model consisted of a human brain, cerebrospinal fluid, and a skull, while the second model contained a human brain, cerebrospinal fluid, a skull, foam padding, and a helmet. These simulations can be broken down into several parts. The first part is a model validation study with data from literature on an unprotected human head. Results are compared to similar simulations which were carried out at three different magnitudes of TNT. This validation provides a basis for the rest of the simulations. The second part describes a model similar to the one used to validate the unprotected head model. However, it includes new material properties for the human skull which were calculated using Mori-Tanaka based homogenization of the porous cancellous bone. This part includes a front and rear impact of a shock wave with three different magnitudes of TNT. The third model incorporates a helmet into the head model. The material properties of the helmet are those used in Advanced Combat Helmets which was described in Chapter 3. The fourth part provides an analysis of the same head-helmet model, with novel nano-composite materials for the helmet. These properties were obtained using Mori-Tanaka homogenization of the original helmet material as a matrix and carbon nanotubes as a fiber material, and were discussed previously.

4.6.1 Numerical Simulation of Unprotected Head Model

Chafi et al. performed an analysis on the human head with the same properties derived earlier, except with a skull of density 1800 kg/m^3, Young's modulus of 15 GPa, and Poisson's ratio of 0.21 [39]. They studied the effects on the brain and the impact due to different amounts of TNT namely, 0.0838, 0.205, and 0.5 lbs (0.038, 0.093, and 0.227 kg) at a stand-off distance of

80 cm from the explosion. The peak maximum shear stress at the coup side for each amount of TNT was determined.

The three different magnitudes of explosion were modeled using the CONWEP blast loading. Figure 4.7 demonstrates the pressure waves at the front of the skull applied by CONWEP blast loading at a distance of 0.8 m in front of the head model.

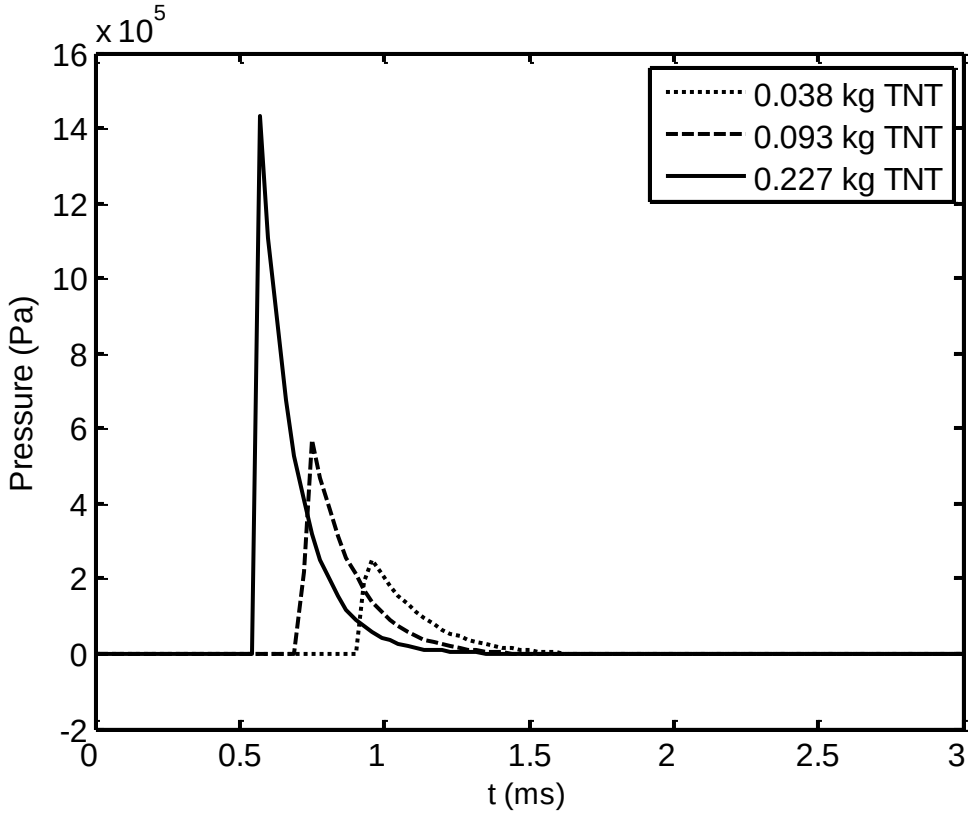

Figure 4.7: CONWEP pressure applied at front of skull.

The coup side corresponds to the site of impact with the explosion; in this case, the front of the brain. For the 0.0838 lb scenario, the maximum shear stress was found to be 23.2 kPa and with 0.295 lb of TNT, the maximum shear stress was obtained as 53.4 kPa. For a 0.5 lb explosion, the maximum shear stress was obtained as 90.9 kPa. Table 4.1 demonstrates the comparisons between Chafi's simulations and those performed in this work.

Table 4.1: Maximum shear stress comparisons

Model	0.038 kg TNT	0.093 kg TNT	0.227 kg TNT
Chafi et al.	19.5 kPa	32.1 kPa	60.9 kPa
Current Work	23.2 kPa	53.4 kPa	90.9 kPa

The differences between the new head model and Chafi's model may be attributed to slight material property variations, boundary conditions, and the use of an Eulerian-Lagrangian mixed model in their simulations. However, the results obtained by the new head model can be said to be validated by those obtained by Chafi et al. The coup shear stress for the brain for the three different explosions, measured with respect to time is indicated in Figure 4.8.

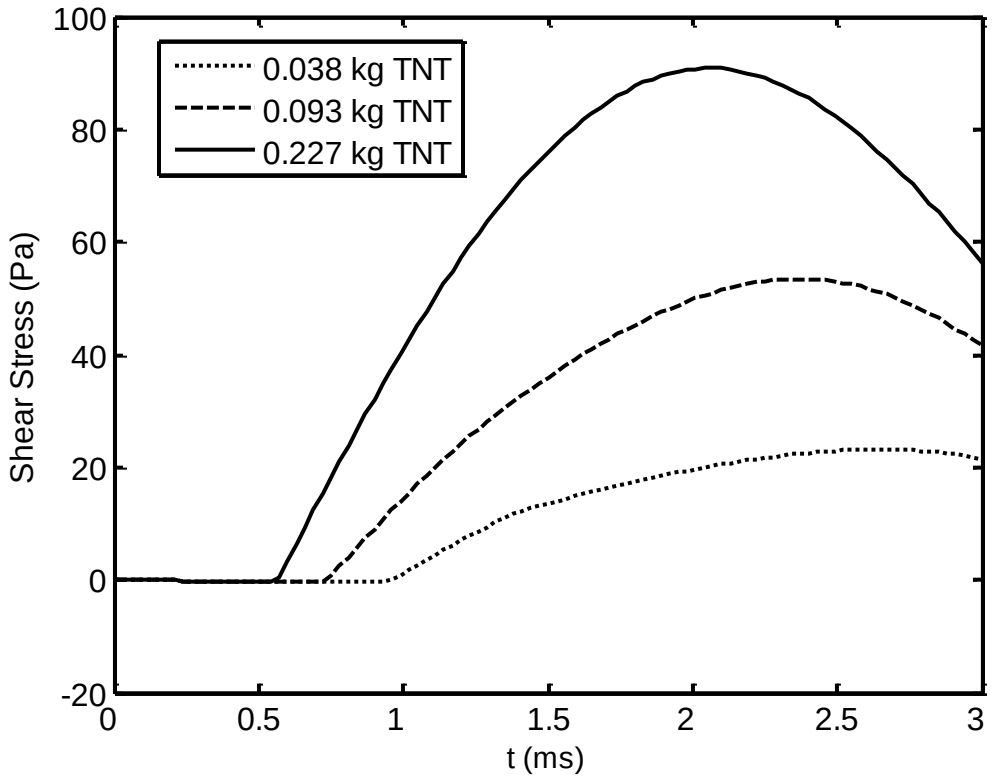

Figure 4.8: Shear stress for the unprotected head model at the front of the brain.

In the remainder of the simulations, the maximum principal stress will be used to express the stress at different points on the head model. Figure 4.9 demonstrates the maximum principal stress experienced by the front of the skull for the three different magnitudes of explosion.

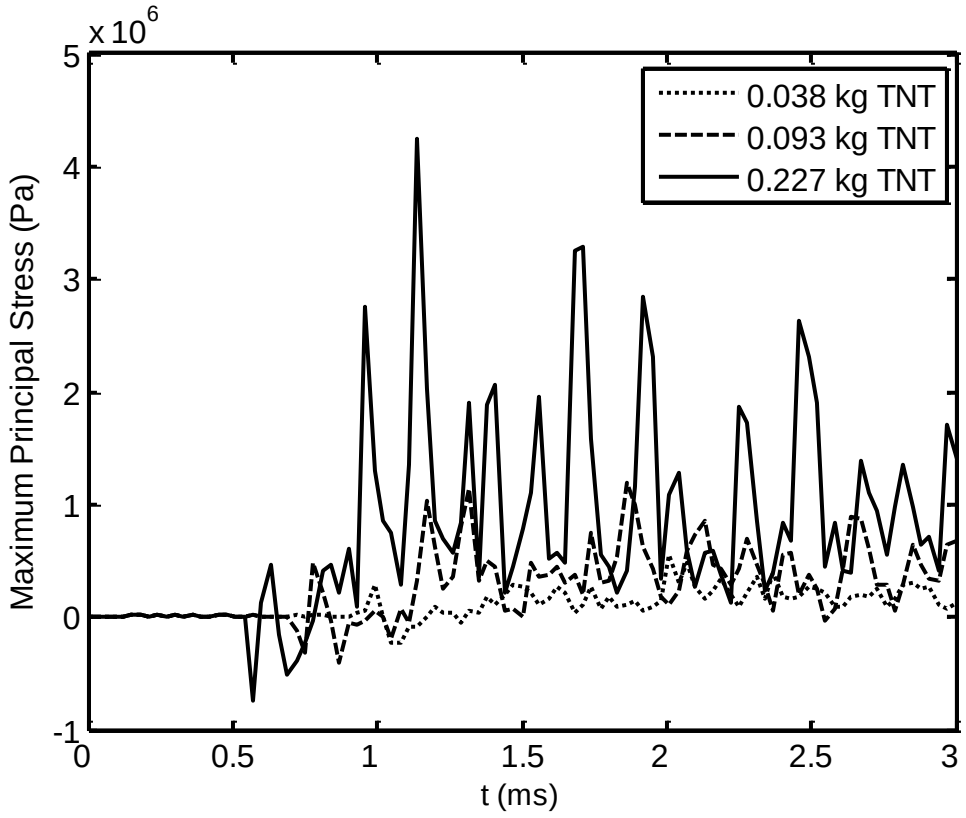

Figure 4.9: Maximum principal stress at the front of the skull model.

4.6.2 Improved Unprotected Head Model

The verification model used the properties discussed in Chapter 3, except for the properties of the skull material. Another simulation was carried out with the new skull material properties derived using Mori-Tanaka homogenization discussed previously. It is proposed that the skull with the homogenized material properties is a better model than the one used by Chafi et al. because it takes into account the porosity of the cancellous skull bone and thus creates a more realistic linear elastic skull material model. Figure 4.10 demonstrates the maximum shear stress at the brain for the M-T-homogenized model.

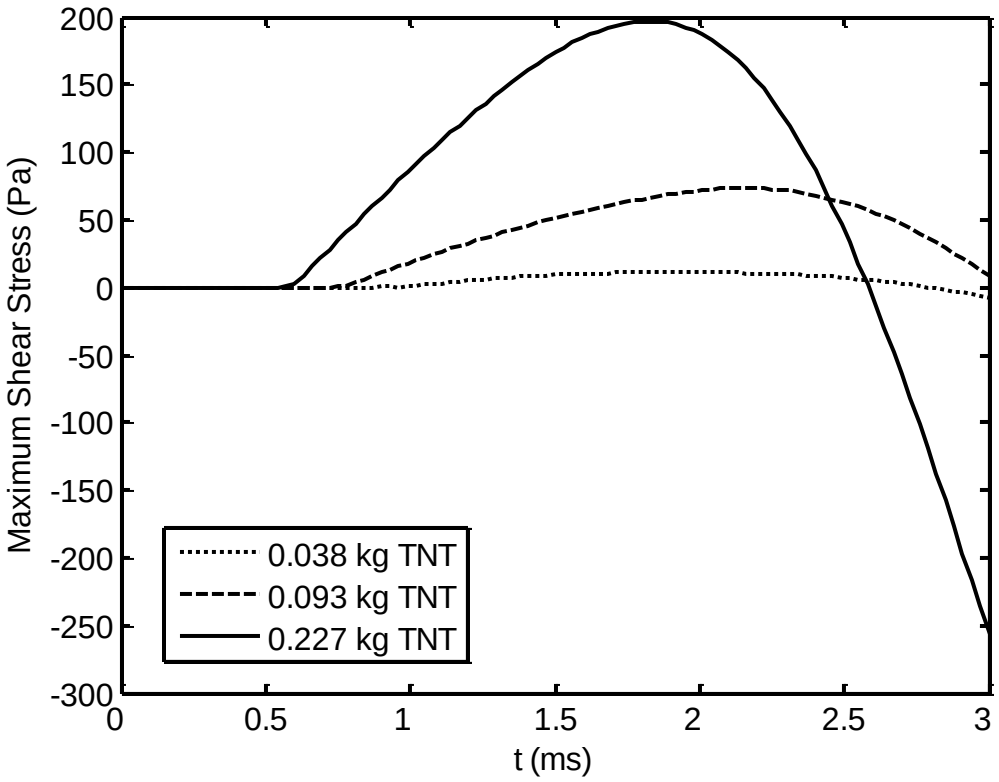

Figure 4.10: Maximum shear stress for the new head model.

Table 4.2 demonstrates the changes in maximum shear stress in the brain at the coup site due to the change in material properties.

Table 4.2: Maximum shear stress comparisons

Material Model	**0.038 kg TNT**	**0.093 kg TNT**	**0.227 kg TNT**
Chafi et al. skull	23.2 kPa	53.4 kPa	90.9 kPa
M-T skull	11.2 kPa	73.4 kPa	196.9 kPa

The differences are due to the different mechanical properties used in the skull material model. There are many other head models which have been used in the past. The main purpose of this work is to present a model for a helmet which will mitigate the effects of blast wave impacts on the human head causing traumatic brain injury. The remainder of the analysis will focus on the use of helmets in mitigating the effects of blast wave impacts. It is proposed that as

long as the stress experienced at the brain is minimized, the results will be valid, regardless of the validity of the skull material model. Future work will need to consider whether the Mori-Tanaka homogenization of the skull material is useful as a means of simulating the porous nature of the skull bone. Figure 4.11 demonstrates the unprotected head model and its cross-section view.

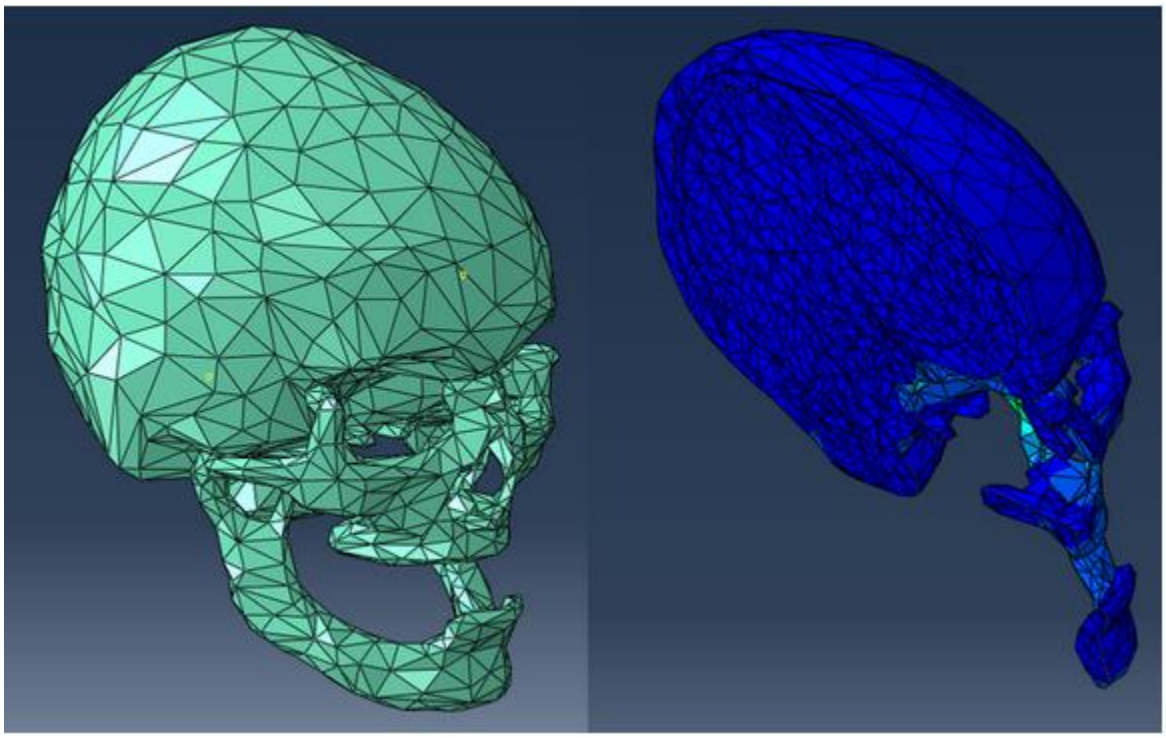

Figure 4.11: Unprotected head with its cross-section.

The shear stress at the coup site for the three different explosion sizes using the M-T homogenization of the skull material is shown in Figure 4.12.

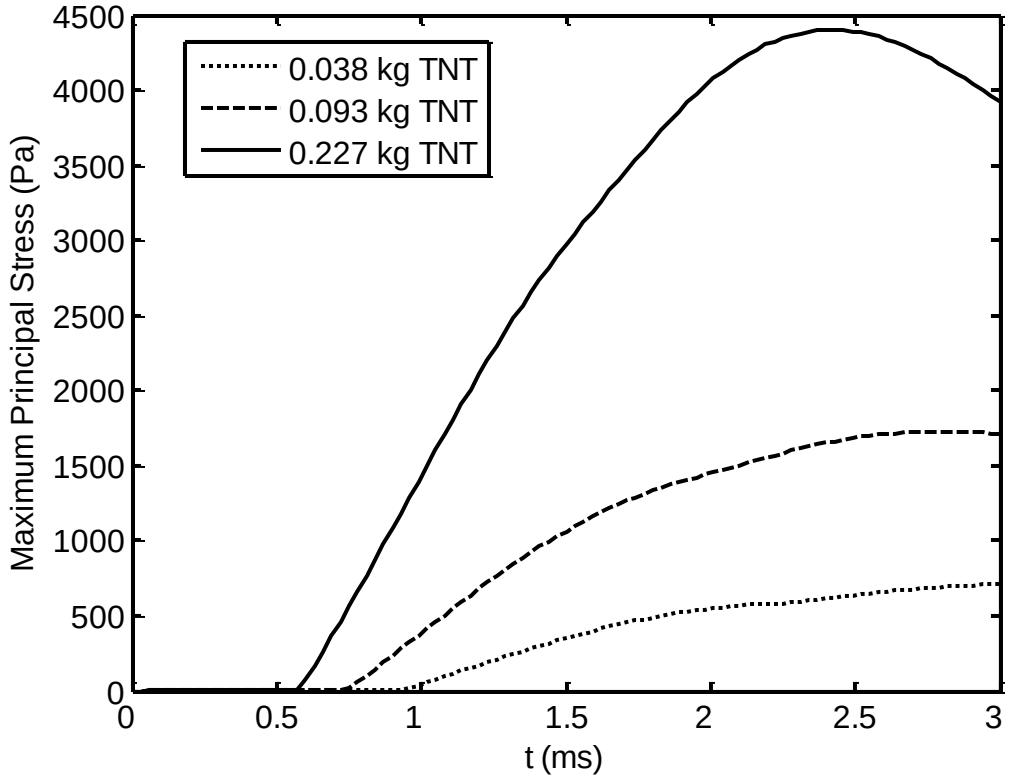

Figure 4.12: Maximum principal stress for the unprotected head model at the front of the brain, with M-T homogenization.

Figure 4.13 demonstrates the maximum principal stress distribution at the point of impact of the pressure wave at the coup site of the brain for the 0.038 kg TNT case for the impact occurring at 0.96 ms.

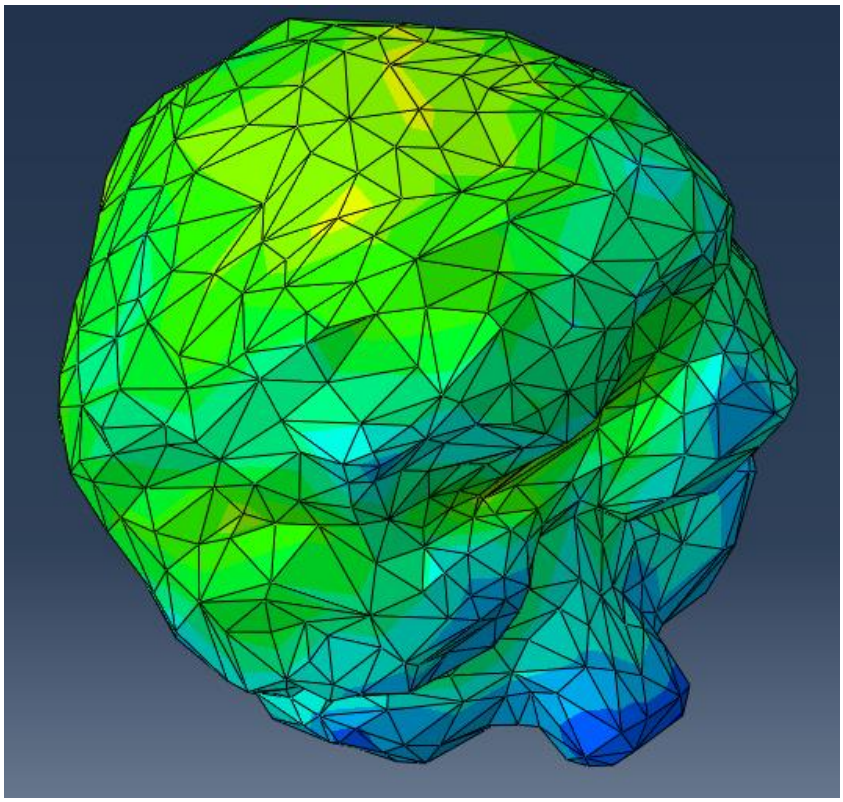

Figure 4.13: Maximum stress at time of impact of pressure wave of 0.038 kg TNT.

The brain also experienced displacement and strain from each of the detonations. Figures 4.14 and 4.15 indicate the displacement and maximum principal strain for each of the three detonations taken at the brain model's coup site.

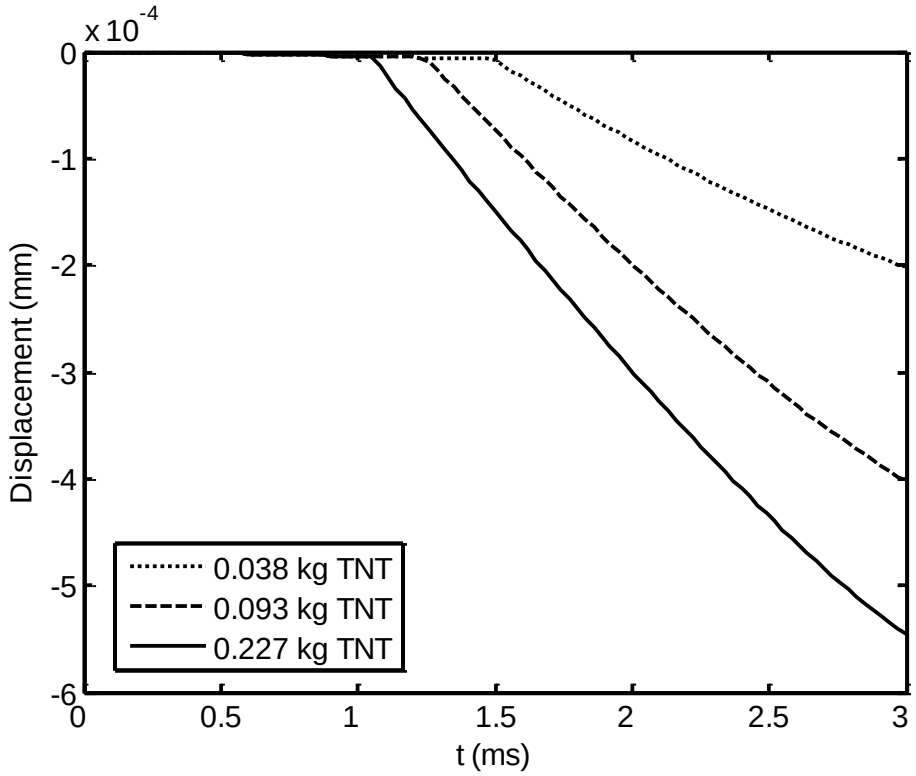

Figure 4.14: Brain displacement for frontal explosions on unprotected head.

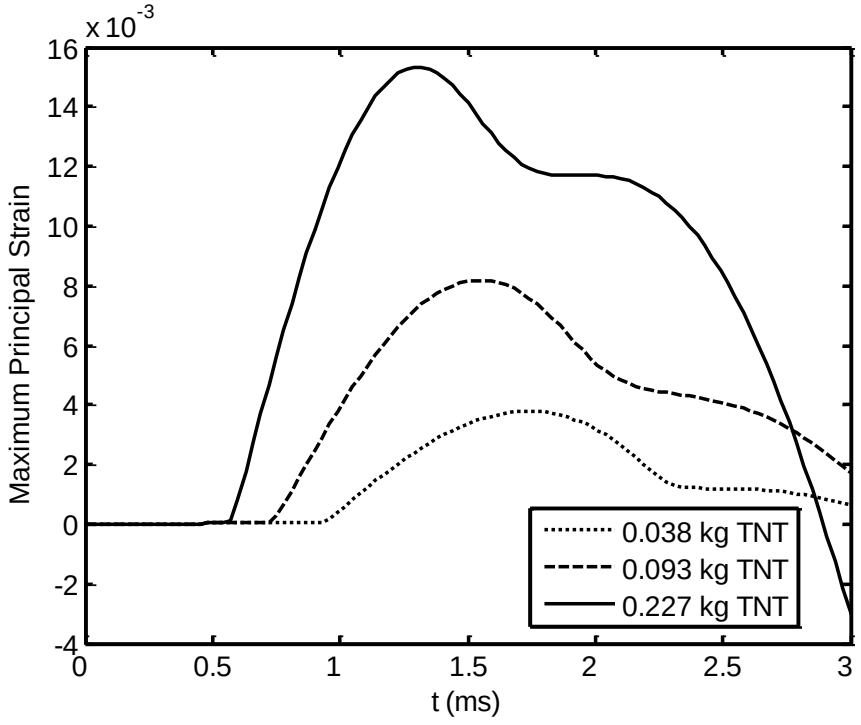

Figure 4.15: Maximum principal strain for unprotected frontal detonations.

The brain experienced stress at the rear, or countercoup site, as well. The countercoup site did not experience the same magnitude of stress increase as the coup site; however, the stress increase is still significant and the increase in maximum principal stress at the countercoup site obtained for each detonation is indicated in Figure 4.16.

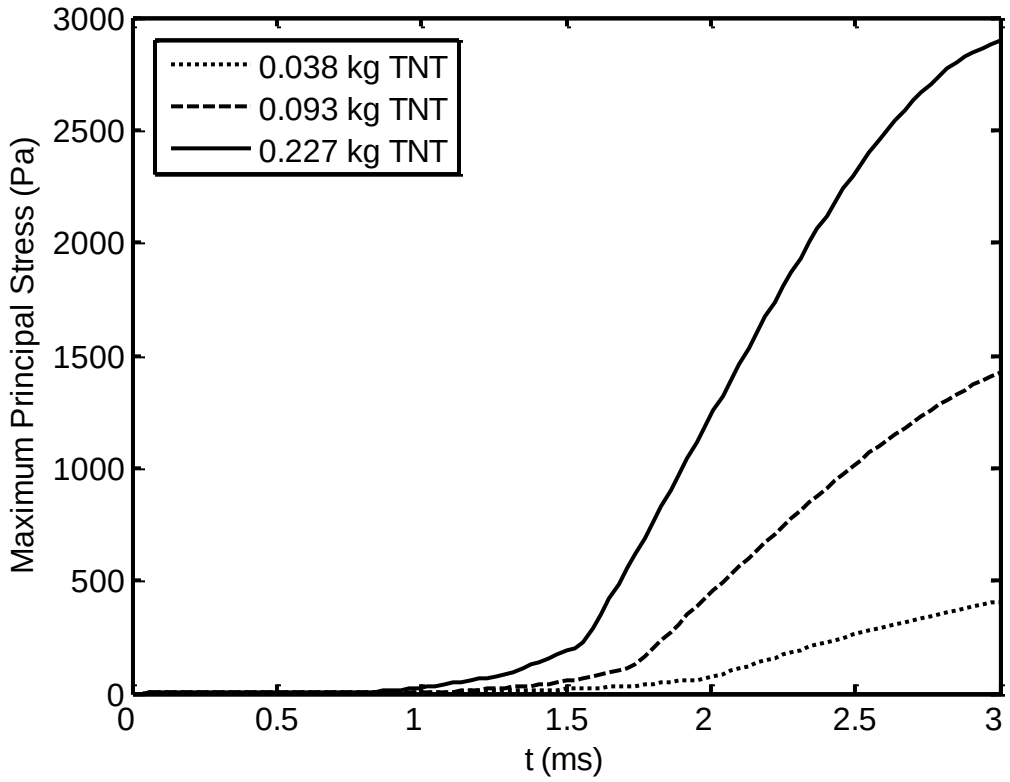

Figure 4.16: Brain countercoup site principal stress for unprotected frontal detonations.

The next simulations performed simulated the same magnitudes of TNT exploding, but at a distance of 0.8 m to the rear of the head. The brain again experienced displacement and strain from each of the detonations. The roles of the coup and countercoup sites are reversed, since the detonation is now performed at the rear of the head. Figures 4.17, 4.18, 4.19, and 4.20 demonstrates the maximum principal stress at the coup and countercoup sites, displacement, and maximum principal strain for each of the three detonations taken at the brain model's coup site.

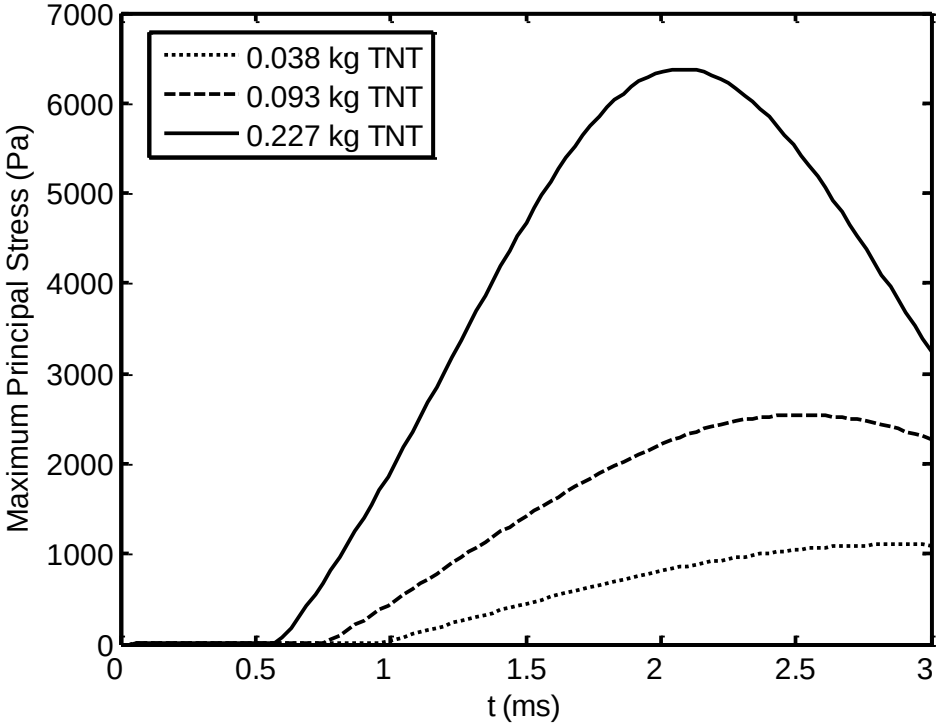

Figure 4.17: Brain coup site principal stress for unprotected rear detonations.

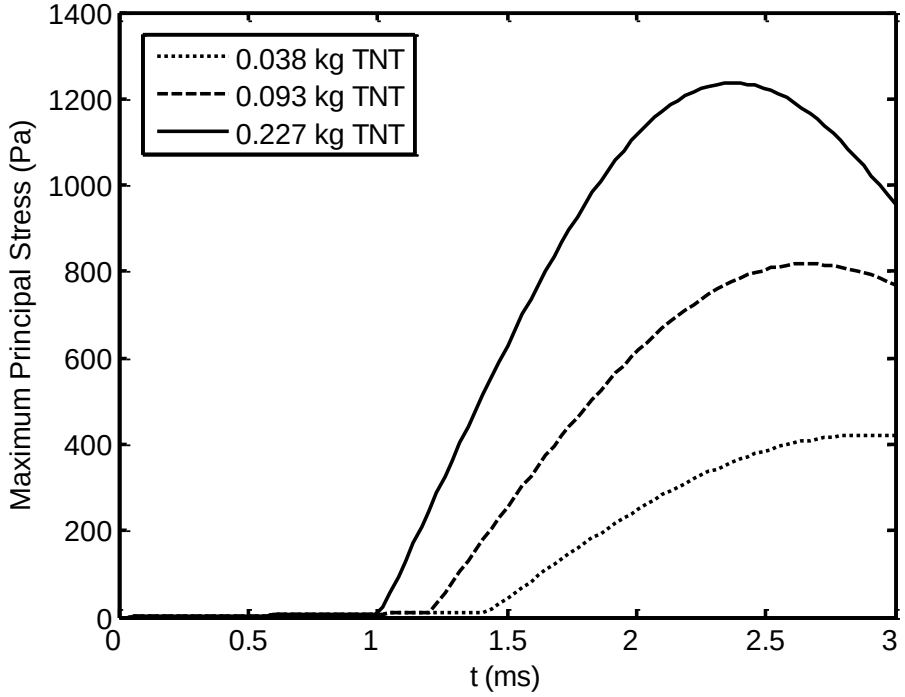

Figure 4.18: Brain countercoup site principal stress for unprotected rear detonations.

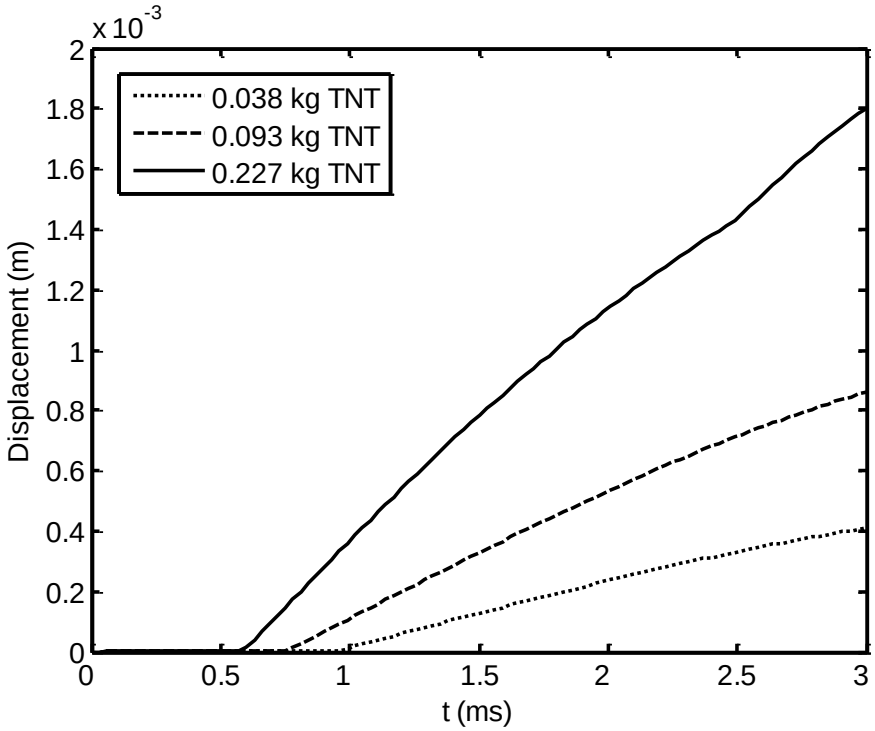

Figure 4.19: Brain displacement for rear explosions on unprotected head.

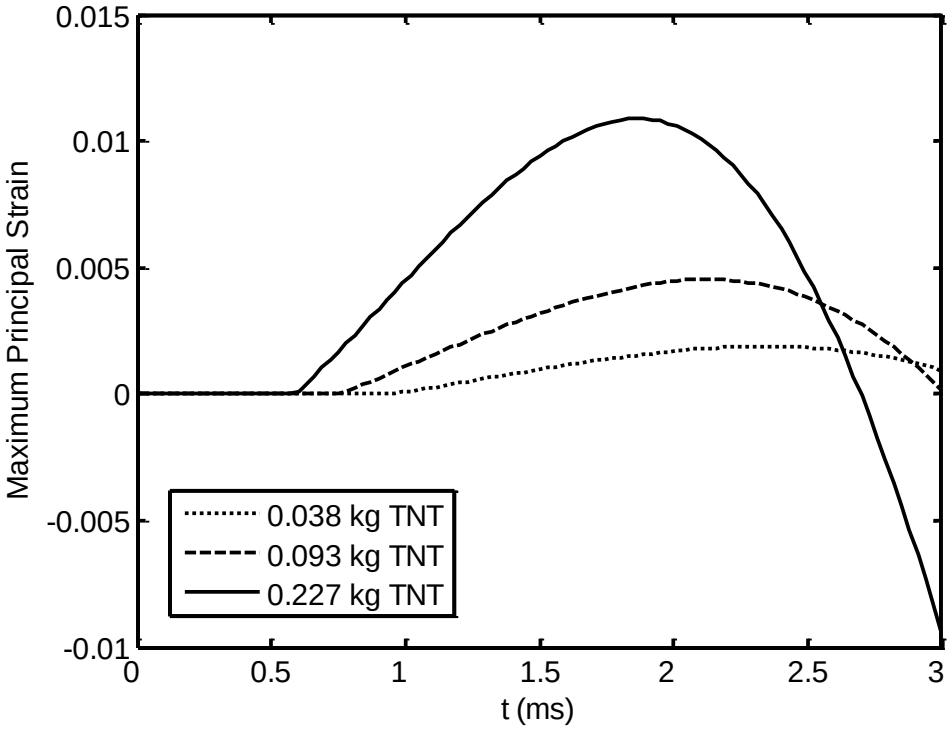

Figure 4.20: Maximum principal strain for unprotected rear detonations.

A helmet was then added to the head model. Similar simulations were carried out to demonstrate the efficacy of the helmet in mitigating the effects of shock waves impacting the human head. The results obtained from detonations occurring at the front of the head will be discussed and compared to those obtained on an unprotected head model. Figure 4.21 demonstrates the addition of a helmet to the model.

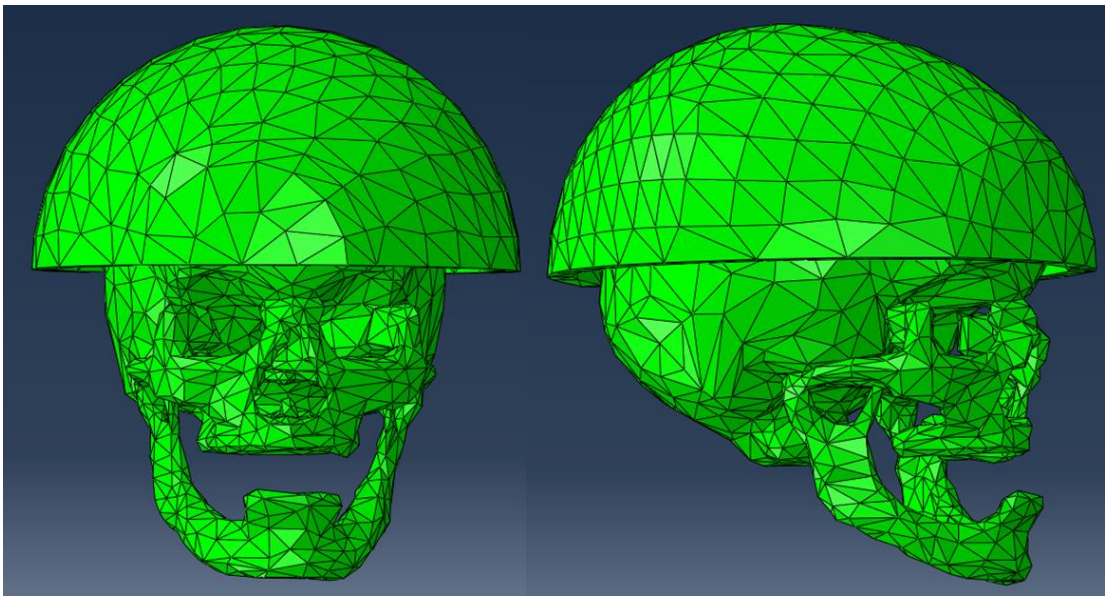

Figure 4.21: Head-helmet finite element model.

The helmet includes padding on the inside, which is visible in Figure 4.22. This demonstrates the mesh of the helmet and inside padding, along with the mesh of the head model.

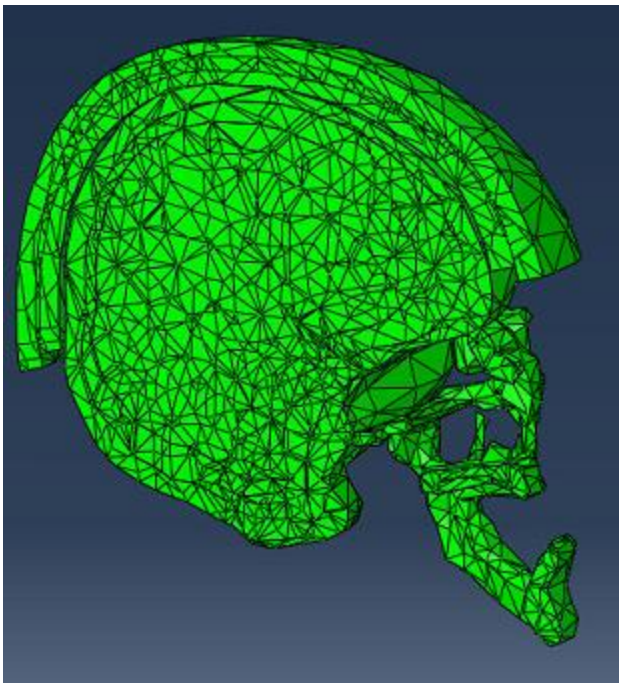

Figure 4.22: Cross section of the head-helmet model.

The different magnitudes of the maximum principal stress were obtained and are compared in Figure 4.23.

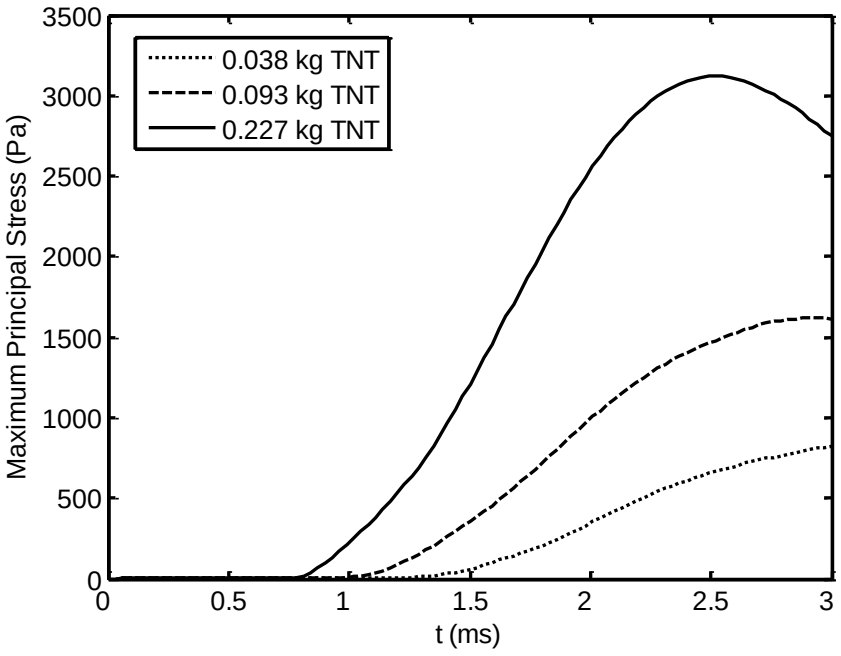

Figure 4.23: Maximum principal stress for the head with the Advanced Combat Helmet.

The results were also compared with the unprotected head model. The results are shown in Figure 4.24.

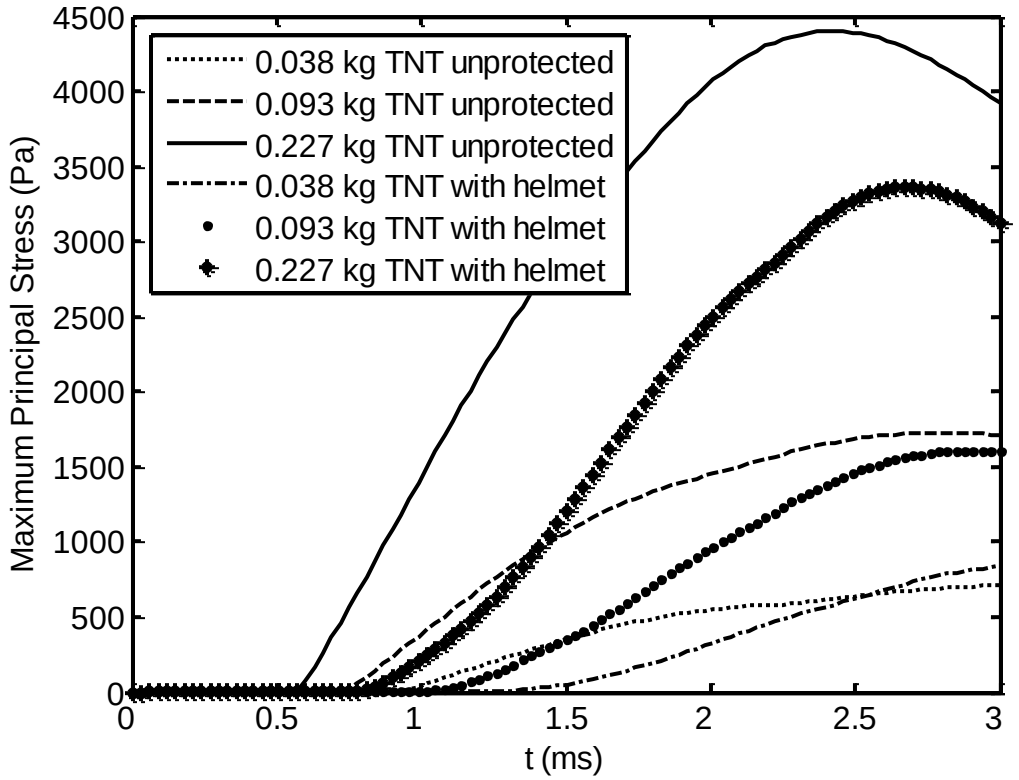

Figure 2.24: Maximum principal stress with and without protection from a helmet.

The results obtained show that at the highest load of 0.227 kg TNT, the maximum principal stress is significantly reduced compared to the unprotected head. The middle load of 0.093 kg of TNT is not much different than the unprotected head, while the lowest load of 0.038 kg of TNT is slightly higher than that which was measured for the unprotected head. This can be attributed to the possibility of taking the measurements at a different element in each model, causing experimental error.

The final simulations used the same helmet-head model, with the new properties for a carbon nanotube-infused thermoset resin/Kevlar®K129 helmet discussed and derived previously.

The same blast loads were applied to this head model and the results are compared in Figure 4.25.

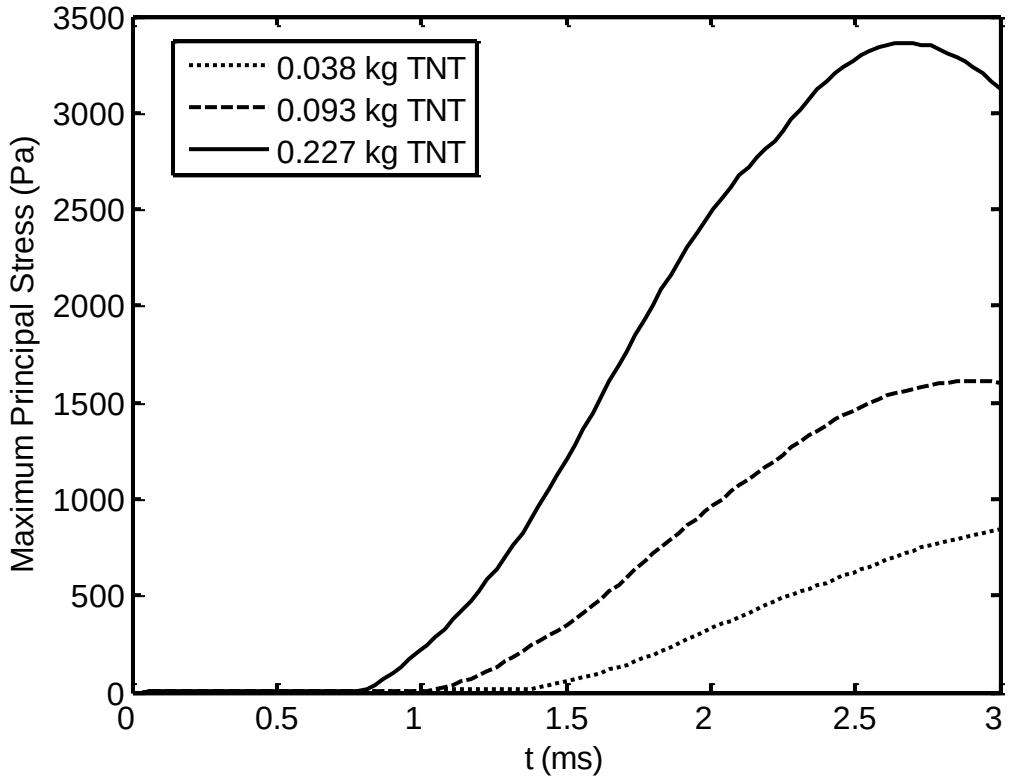

Figure 4.25: Maximum principal stress for helmet-head model using a new material for helmet.

Table 4.3 compares the maximum values of principal stress obtained for the frontal simulations on the unprotected head, the head protected with an Advanced Combat Helmet, and the head protected with a helmet using the new material properties. The new material proposed did mitigate the effects of the blast wave on the brain; however, it did not perform better than the current material used in the helmet. Increasing the amount of carbon nanotube fibers may make the helmet better; however, this is difficult to do in an industrial setting and is also very costly. Running the simulations with higher percentages of carbon nanotube fibers incorporated into the thermoset resin/Kevlar®K129 (50%) produced improved results; however, these results were not

realistic due to the aforementioned difficulty in obtaining such high percentages of carbon nanotubes.

Table 4.3: Comparison of the maximum principal stresses.

TNT	Unprotected head	Head with ACH	Head with CNT helmet
0.038 kg	709.66 Pa	818.89 Pa	839.65 Pa
0.093 kg	1729.3 Pa	1619.0 Pa	1609.7 Pa
0.227 kg	4401.8 Pa	3119.9 Pa	3360.9 Pa

The results indicate that the head with a carbon nanotube-enhanced helmet was more protected than the head with the original ACH helmet only in the case of the 0.093 kg TNT blast. In all other blasts it exhibited a decrease in the ability to mitigate the effects of the pressure wave. This discrepancy may be described by the fact that energy dissipation characteristics are not taken into consideration for the helmet material models, but only an enhancement in the material stiffness due to the CNT is considered in the study. Additionally, the millisecond time scales used in these simulations do not give enough time for the viscous effects of the brain material to be significant. A larger time scale would see more of the realistic viscoelastic responses of the brain tissue. This study was however primarily concerned with mitigating the effects of the initial overpressure shock wave impacting the head.

The decrease in performance for the head with the CNT-enhanced helmet may be described in terms of the specific energy. Specific energy is the amount of energy stored per unit mass and is calculated by dividing the Young's Modulus by the density. The specific energy for the original ACH helmet material was calculated to be 86.1 kJ/kg, whereas the CNT-enhanced helmet material had a specific energy of 96 kJ/kg. Future works may consider the viscoelastic and energy dissipation effects of the materials, together with the capability of the brain to swell and suffer further damage in severe cases of bTBI. Another aspect which has not been discussed is the time at which the maximum stress occurs as each of the models experience maximum

stresses at different times for different magnitudes of TNT charge. The effect of increase in mesh density is also not considered, which can have a significant impact on the computations.

4.6.3 Discussion on Energy Density

The efficacy of the helmet in protecting the brain from bTBI can be measured in terms of the strain energy density. Strain energy density is the amount of strain energy stored per unit volume. Simulations were performed to calculate the energy density for the three different magnitudes of explosions. Figures 4.26, 4.27, and 4.28 indicate the energy density at the front of the brain (coup site) for the porous unprotected head model (M-T model skull), the head protected by the ACH, and the head protected by the CNT-enhanced helmet.

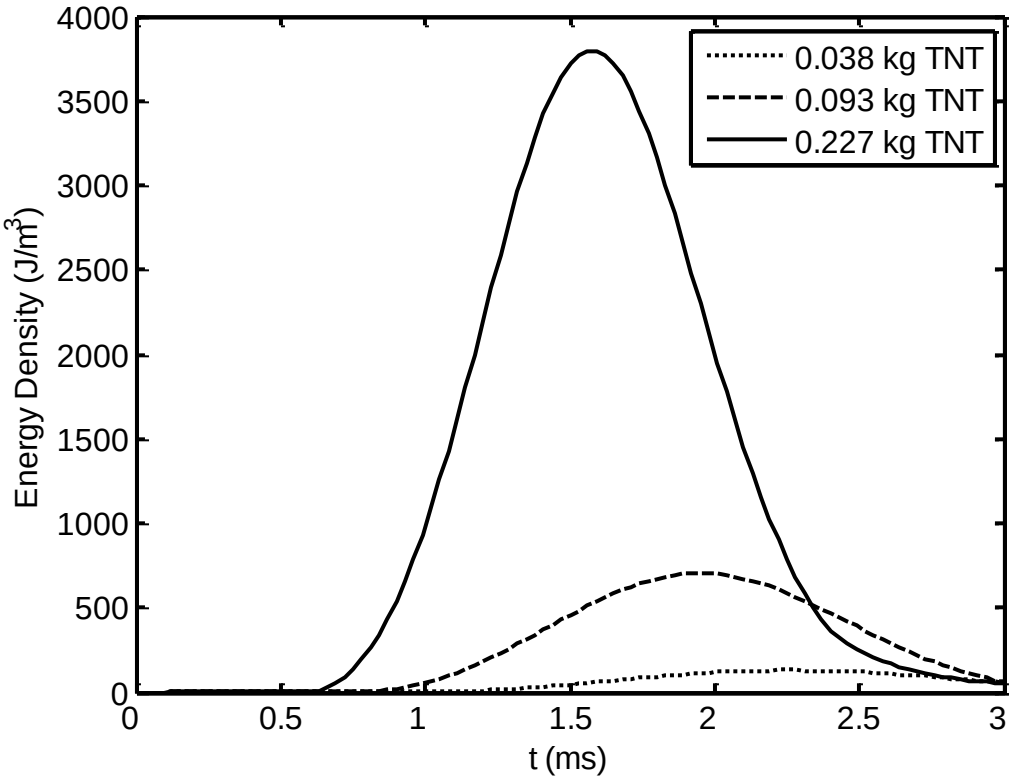

Figure 4.26: Energy density at the brain for the unprotected head model.

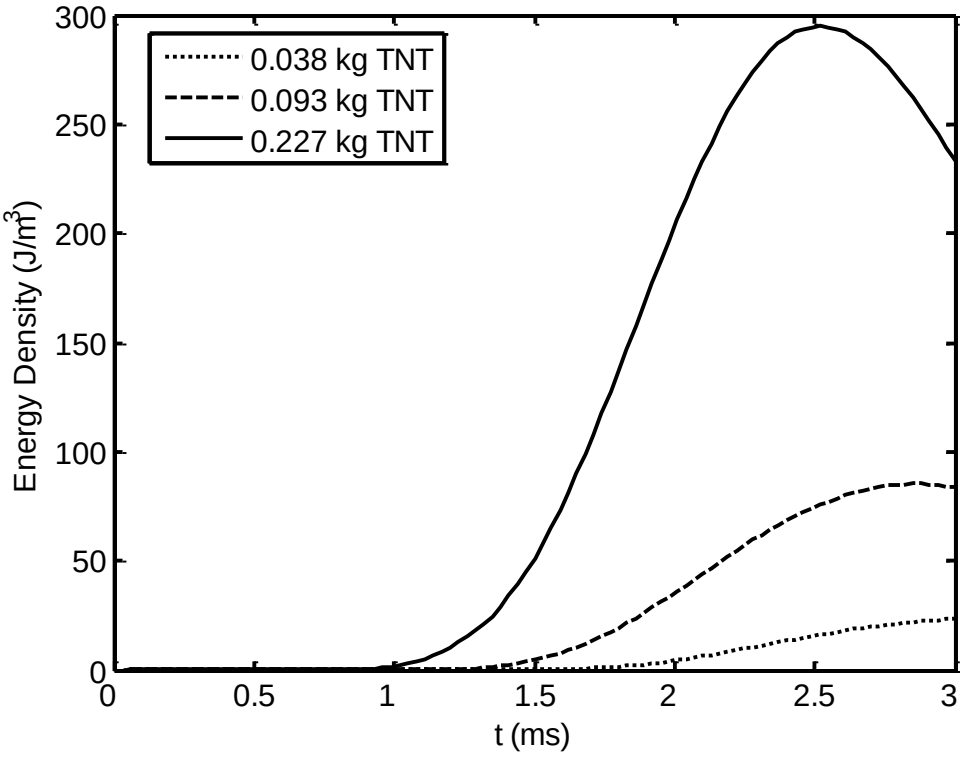

Figure 4.27: Energy density at the brain for the ACH-protected head model.

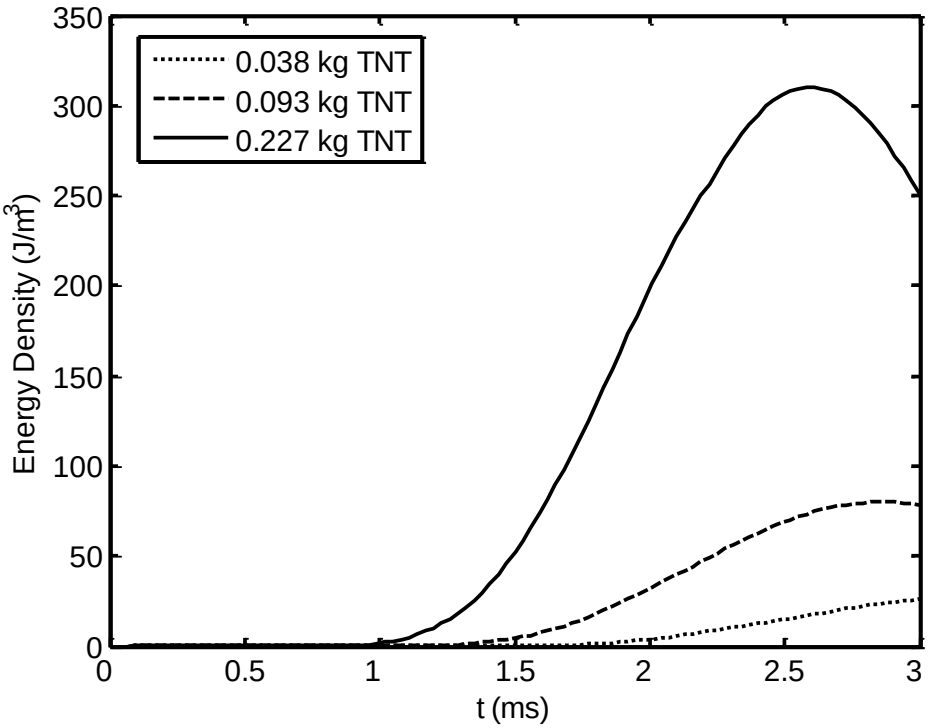

Figure 4.28: Energy density at the brain for the CNT-enhanced protected head model.

Table 4.4 demonstrates a comparison of the maximum energy density for each of the different combinations of detonations.

Table 4.4: Energy Density Comparison.

TNT	Unprotected head	Head with ACH	Head with CNT helmet
0.038 kg	130.56 J/m^3	23.48 J/m^3	25.89 J/m^3
0.093 kg	703.76 J/m^3	85.31 J/m^3	79.93 J/m^3
0.227 kg	3797.6 J/m^3	294.89 J/m^3	310.19 J/m^3

It can be seen that the energy density was greatly reduced when the unprotected head is compared to the head with the advanced combat helmet and the carbon nanotube-enhanced helmet material. This indicates that significant energy is absorbed by the helmet and less shock energy per unit volume is reaching the brain. However, the same discrepancies discussed previously are seen when comparing the CNT-enhanced helmet with the original ACH. Using an energy dissipation based material model can significantly affect this discrepancy.

4.7 Conclusion

This chapter discussed a simulation to model the blast impact on a solid steel plate. This served as a method to verify the results obtained using the ConWep blast loading in Abaqus to ensure a valid simulation in the subsequent head models. The results obtained in this verification study were compared with an experimental investigation in literature. Other materials were also incorporated into the plate model, to perform preliminary tests on novel materials that could perform better in mitigating blast shock wave impacts and compare the current materials used in military helmets.

The human head model was then subjected to blast impacts, and comparisons were made between a head protected by a ballistic helmet and an unprotected head. The obtained results were compared with literature. The performance of new materials for the improvement of the

helmet in mitigating blast shock wave impacts was also studied using the same head-helmet model with different material properties. The results indicate that a carbon nanotube-enhanced ACH does not improve the current version used in military applications.

CHAPTER 5 – CONCLUSION AND FUTURE WORKS

5.1 Conclusion

The focus of this work was to study the effect of the ballistic helmet on mitigating the effects of blast traumatic brain injury using a multiscale analysis of a human head-helmet model. Insight was provided into what is lacking in the current knowledge of the effects of blast shock waves and their interactions with the human head and possible helmet protection systems. Various methods from the current literature were used and new methods devised in the creation of a valid head-helmet model for the analytical finite element study of bTBI. Some important concepts were described, including the Friedlander equation for estimating blast impact incident pressure, the Mooney-Rivlin hyperelastic model for simulating brain properties, and the Mori-Tanaka method for the homogenization of porous microstructures.

In order to validate the results obtained by using ConWep blast loading in Abaqus, a simulation was performed on a steel plate. The results were compared to results obtained in various experimental efforts obtained from literature. Other materials were also incorporated into the plate model, to perform preliminary tests on possible materials that could be better in mitigating blast shock wave impacts. The head model was then subjected to blast impacts and comparisons were made between a head protected by a helmet and an unprotected head. These results are also compared to the literature for validity. Various materials for the improvement of the helmet in mitigating blast shock wave impacts were also tested using the same model with different material properties.

5.2 Future Work

This study was focused on the initial shock wave, while other studies should be done in the future to perform an Eulerian and Lagrangian formulation to study the effects of the high-velocity wind [2]. The complexity of the experimentation and finite element models will be increased, but more valid results will be obtained.

Another future study could be made to include the secondary, tertiary, quaternary, and other injuries listed previously. This work was focused on the initial blast wave impacting the head.

The mesh also could be refined. The original mesh size was much smaller until it had to be simplified due to the length of time to perform the analysis. The head model originally contained 147288 nodes total. The skull model contained 5998 elements, the cerebral spinal fluid model contained 236237 elements, and the brain model contained 230551 elements, for a model total of 718587 elements in the model of the head. An improved head model could be made from more complete MRI or CT scan data. This would allow the study of different portions of the brain and the way they interact to blast waves. Figure 5.1 demonstrates an increased number of elements for the mesh of the skull model.

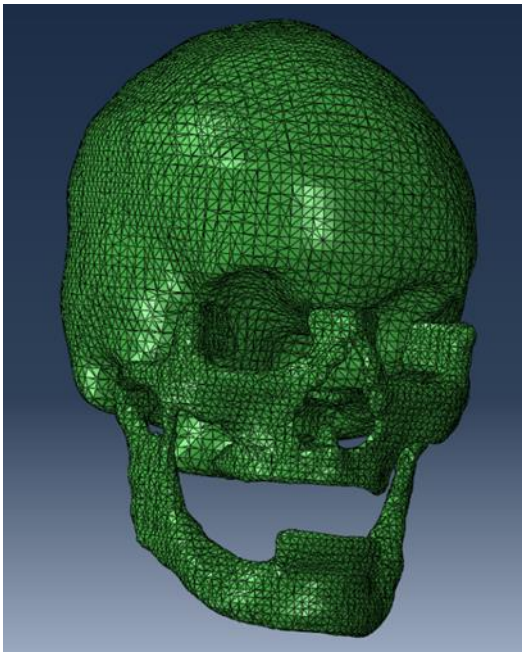

Figure 5.1: Decreased element size for a more refined mesh.

The addition of a visor or goggles could help mitigate the pressure waves entering through the face. This needs to be studied in order to enable the utilization of better materials for use in shielding the face from the pressure impacts, thus reducing the risk of bTBI.

Others have performed finite element analyses on the effects of ballistic helmets in preventing shrapnel impact [17]. The shrapnel analyses performed in previous studies could be compared to new shrapnel impacts performed on the current head-helmet model. An analysis could then be performed to ensure that new materials which possibly mitigate blast impacts are also useful for the prevention of traumatic brain injury due to shrapnel impact. Trading blast impact mitigation for shrapnel impact mitigation would not be a beneficial development.

Further analysis may also be performed using molecular dynamics and micromechanics to enable the simulation and estimation of the mechanical properties of other carbon nanotube-reinforced composite materials to be included in the multiscale analysis and provide the material properties for a FE analysis of the helmet protecting a head. This would possibly lead to

improved results or structures for the mitigation of shock impact on the human head and the prevention of blast-induced traumatic brain injury.

REFERENCES

1. Mellor, A.J. and D. Woods, *Serum neutrophil gelatinase–associated lipocalin in ballistic injuries: A comparison between blast injuries and gunshot wounds.* Journal of Critical Care, 2012. **27**(4): p. 419.e1-419.e5.

2. Kulkarni, S.G., et al., *Ballistic helmets – Their design, materials, and performance against traumatic brain injury.* Composite Structures, 2013. **101**(0): p. 313-331.

3. Kumar, P., et al., *Effect of plate curvature on blast response of aluminum panels.* International Journal of Impact Engineering, 2012. **46**(0): p. 74-85.

4. Alley, M.D., B.R. Schimizze, and S.F. Son, *Experimental modeling of explosive blast-related traumatic brain injuries.* NeuroImage, 2011. **54, Supplement 1**(0): p. S45-S54.

5. Jones, C., *Glasgow coma scale.* AJN The American Journal of Nursing, 1979. **79**(9): p. 1551-1557.

6. Ghajar, J., *Traumatic brain injury.* The Lancet, 2000. **356**(9233): p. 923-929.

7. Alley, M.D., B.R. Schimizze, and S.F. Son, Experimental Modeling of Explosive Blast Related Traumatic Brain Injuries., 2010. **1**: p. 45-54.

8. Courtney, A.C. and M.W. Courtney, *A thoracic mechanism of mild traumatic brain injury due to blast pressure waves.* Medical Hypotheses, 2009. **72**(1): p. 76-83.

9. Lee, K.Y., et al., *Blast-induced electromagnetic fields in the brain from bone piezoelectricity.* Neuroimage, 2010. **54**(SUPPL. 1): p. 30-36.

10. Baker, W.E., *Explosions in air*. 1973: University of Texas Press Austin.

11. Flynn, P., *Elastic response of simple structures to pulse loading.* Ballistics Research Laboratory, Aberdeen Proving Ground, Maryland, USA, BRL Memo Report, 1950(525).

12. Ethridge, N., *A Procedure for Reading and Smoothing Pressure-Time Data from HE and Nuclear Explosions*. 1965: Army. Ballistic Research Laboratories.

13. Tan, K.T., H.H. Huang, and C.T. Sun, *Blast-wave impact mitigation using negative effective mass density concept of elastic metamaterials.* International Journal of Impact Engineering, 2014. **64**(0): p. 20-29.

14. Dewey, J.M. *The shape of the blast wave: studies of the Friedlander equation*. in *International Symposium on Military Aspects of Blast and Shock, Jeruzalem, Israel*. 2010.

15. Kingery, C.N. and G. Bulmash, *Air blast parameters from TNT spherical air burst and hemispherical surface burst*. 1984: Ballistic Research Laboratories.

16. Sheng, N. and S. Li, *A non-equilibrium multiscale simulation of shock wave propagation.* Mechanics Research Communications, 2008. **35**(1): p. 10-16.

17. Aare, M. and S. Kleiven, *Evaluation of head response to ballistic helmet impacts using the finite element method.* International Journal of Impact Engineering, 2007. **34**(3): p. 596-608.

18. Ganpule, S., et al., *Role of helmet in the mechanics of shock wave propagation under blast loading conditions.* Computer Methods in Biomechanics and Biomedical Engineering, 2011. **15**(11): p. 1233-1244.

19. Chavko, M., et al., *Measurement of blast wave by a miniature fiber optic pressure transducer in the rat brain.* Journal of neuroscience methods, 2007. **159**(2): p. 277-281.

20. Zhang, J., et al., *Experimental study of blast-induced traumatic brain injury using a physical head model.* Stapp car crash journal, 2009. **53**: p. 215.

21. Bauman, R.A., et al., *An introductory characterization of a combat-casualty-care relevant swine model of closed head injury resulting from exposure to explosive blast.* Journal of Neurotrauma, 2009. **26**(6): p. 841-860.

22. Kleiven, S. and H. von Holst, *Consequences of Reduced Brain Volume Following Impact in Prediction of Subdural Hematoma Evaluated with Numerical Techniques.* Traffic Injury Prevention, 2002. **3**(4): p. 303-310.

23. M. Grujicic, G.A., T. He, *Material-modeling and structural-mechanics aspects of the traumatic brain injury problem.* Multidiscipline Modeling in Materials and Structures, 2010. **6**(3): p. 335-363.

24. El Sayed, T., et al., *Biomechanics of traumatic brain injury*. Computer Methods in Applied Mechanics and Engineering, 2008. **197**(51-52): p. 4692-4701.

25. Vonach, M., et al., *A method for rapid production of subject specific finite element meshes for electrical impedance tomography of the human head.* Physiological Measurement, 2012. **33**(5): p. 801.

26. Keyak, J.H., et al., *Automated three-dimensional finite element modelling of bone: A new method.* Journal of Biomedical Engineering, 1990. **12**(5): p. 389-397.

27. Chen, Y. and M. Ostoja-Starzewski, *MRI-based finite element modeling of head trauma: Spherically focusing shear waves.* Acta Mechanica, 2010. **213**(1-2): p. 155-167.

28. Taylor, P.A. and C.C. Ford, *Simulation of blast-induced early-time intracranial wave physics leading to traumatic brain injury.* Journal of biomechanical engineering, 2009. **131**(6): p. 061007.

29. Miller, K., *Constitutive model of brain tissue suitable for finite element analysis of surgical procedures.* Journal of Biomechanics, 1999. **32**(5): p. 531-537.

30. Zhang, J., et al., *Viscoelastic properties of human cerebellum using magnetic resonance elastography.* Journal of Biomechanics, 2011. **44**(10): p. 1909-1913.

31. Miller, K. and K. Chinzei, *Mechanical properties of brain tissue in tension.* Journal of Biomechanics, 2002. **35**(4): p. 483-490.

32. Brands, D.W.A., G.W.M. Peters, and P.H.M. Bovendeerd, *Design and numerical implementation of a 3-D non-linear viscoelastic constitutive model for brain tissue during impact.* Journal of Biomechanics, 2004. **37**(1): p. 127-134.

33. Zhang, J., et al., *Experimental model for civilian ballistic brain injury biomechanics quantification.* Journal of Biomechanics, 2007. **40**(10): p. 2341-2346.

34. Arbogast, K.B. and S.S. Margulies, *Material characterization of the brainstem from oscillatory shear tests.* Journal of biomechanics, 1998. **31**(9): p. 801-807.

35. Shuck, L. and S. Advani, *Rheological response of human brain tissue in shear.* Journal of basic engineering, 1972. **94**(4): p. 905-911.

36. Nicolle, S., M. Lounis, and R. Willinger, *Shear properties of brain tissue over a frequency range relevant for automotive impact situations: new experimental results.* Stapp Car Crash Journal, 2004. **48**: p. 239-258.

37. Velardi, F., F. Fraternali, and M. Angelillo, *Anisotropic constitutive equations and experimental tensile behavior of brain tissue.* Biomechanics and Modeling in Mechanobiology, 2006. **5**(1): p. 53-61.

38. Wright, R.M. and K. Ramesh, *An axonal strain injury criterion for traumatic brain injury.* Biomechanics and modeling in mechanobiology, 2012. **11**(1-2): p. 245-260.

39. Chafi, M., G. Karami, and M. Ziejewski, *Biomechanical assessment of brain dynamic responses due to blast pressure waves.* Annals of biomedical engineering, 2010. **38**(2): p. 490-504.

40. Darvish, K.K. and J.R. Crandall, *Nonlinear viscoelastic effects in oscillatory shear deformation of brain tissue.* Medical Engineering and Physics, 2001. **23**(9): p. 633-645.

41. Grujicic, M., et al., *Blast-wave impact-mitigation capability of polyurea when used as helmet suspension-pad material.* Materials & Design, 2010. **31**(9): p. 4050-4065.

42. Langdon, G.S., et al., *Performance of mild steel perforated plates as a blast wave mitigation technique: Experimental and numerical investigation.* International Journal of Impact Engineering, 2010. **37**(10): p. 1021-1036.

43. Schimizze, B., et al., *An experimental and numerical study of blast induced shock wave mitigation in sandwich structures.* Applied Acoustics, 2013. **74**(1): p. 1-9.

44. Wu, C. and H. Sheikh, *A finite element modelling to investigate the mitigation of blast effects on reinforced concrete panel using foam cladding.* International Journal of Impact Engineering, 2013. **55**(0): p. 24-33.

45. Neuberger, A., S. Peles, and D. Rittel, *Scaling the response of circular plates subjected to large and close-range spherical explosions. Part I: Air-blast loading.* International Journal of Impact Engineering, 2007. **34**(5): p. 859-873.

46. Le Blanc, G., M. Adoum, and V. Lapoujade. *External blast load on structures–Empirical approach*. in *5th European LS Dyna Users Conference, France*. 2005.

47. Ostraich, B., et al., *A method for transforming a full computation of the effects of a complex-explosion scenario to a simple computation by ConWep.* Shock Waves, 2011. **21**(2): p. 101-109.

48. Ackerman, M.J., *Accessing the visible human project.* D-Lib Magazine, 1995. **1**(4).

49. Nguyen, T., *Effects of Curvature on the Stresses of a Curved Laminated Beams Subjected to Bending.* 2010.

50. Tham, C.Y., V.B.C. Tan, and H.P. Lee, *Ballistic impact of a KEVLAR® helmet: Experiment and simulations.* International Journal of Impact Engineering, 2008. **35**(5): p. 304-318.

51. Simulia, D.S., *Abaqus 6.12 documentation.* Providence, Rhode Island, US, 2012.

52. Reuss, A., *Berechnung der Fließgrenze von Mischkristallen auf Grund der Plastizitätsbedingung für Einkristalle.* ZAMM - Journal of Applied Mathematics and Mechanics / Zeitschrift für Angewandte Mathematik und Mechanik, 1929. **9**(1): p. 49-58.

53. Voigt, W., *Theoretische studien über die elasticitätsverhältnisse der krystalle*. 1887: Königliche Gesellschaft der Wissenschaften zu Göttingen.

54. Fisher, F.T., R.D. Bradshaw, and L.C. Brinson, *Fiber waviness in nanotube-reinforced polymer composites I: Modulus predictions using effective nanotube properties.* Composites Science and Technology, 2003. **63**(11): p. 1689-1703.

55. Mura, T., *Micromechanics of Defects in Solids*. 1997, Hague, The Netherlands: Martinus Nijhoff.

56. Unnikrishnan, V.U. and J.N. Reddy, *Characteristics of Silicon Doped Carbon Nanotube Reinforced Nanocomposites.* International Journal for Multiscale Computational Engineering, 2005. **3**(4): p. 437-450.

57. Mori, T. and K. Tanaka, *Average stress in matrix and average elastic energy of materials with misfitting inclusions.* Acta Metallurgica, 1973. **21**(5): p. 571-574.

58. Gilbert, R.P., P. Guyenne, and J. Li, *A viscoelastic model for random ultrasound propagation in cancellous bone.* Computers & Mathematics with Applications, 2013. **66**(6): p. 943-964.

59. Qu, J. and C. Wong. *Effective elastic modulus of underfill material for flip-chip applications*. in *Electronic Components & Technology Conference, 1998. 48th IEEE*. 1998. IEEE.

60. Qu, J., *The effect of slightly weakened interfaces on the overall elastic properties of composite materials.* Mechanics of Materials, 1993. **14**(4): p. 269-281.

61. Bilisik, A.K. and Y. Turhan, *Multidirectional stitched layered aramid woven fabric structures and their experimental characterization of ballistic performance.* Textile Research Journal, 2009. **79**(14): p. 1331-1343.

62. Jason, A.M., *Facial protective devices for blast-induced traumatic brain injury mitigation*. 2010, Massachusetts Institute of Technology.

63. Wharton, R.K., S.A. Formby, and R. Merrifield, *Airblast TNT equivalence for a range of commercial blasting explosives.* Journal of Hazardous Materials, 2000. **79**(1–2): p. 31-39.

64. Johnson, G.R. and W.H. Cook. *A constitutive model and data for metals subjected to large strains, high strain rates and high temperatures*. in *Proceedings of the 7th International Symposium on Ballistics*. 1983. The Netherlands.

65. Stuart, S.J., A.B. Tutein, and J.A. Harrison, *A reactive potential for hydrocarbons with intermolecular interactions.* The Journal of Chemical Physics, 2000. **112**(14): p. 6472-6486.

66. Meo, M. and M. Rossi, *Prediction of Young's modulus of single wall carbon nanotubes by molecular-mechanics based finite element modelling.* Composites Science and Technology, 2006. **66**(11–12): p. 1597-1605.

67. Collins, P.G. and P. Avouris, *Nanotubes for electronics.* Scientific American, 2000. **283**(6): p. 62-69.